Dual transcriptomics to determine interferon-gamma independent host response to intestinal Cryptosporidium parvum infection

Roberta M. O'Connor
Washington State University
Andrés M. Tibabuzo Perdomo
University of Wisconsin–Madison
Andrew L. Garfoot
University of Wisconsin–Madison
Gina M Gallego-Lopez
University of Wisconsin–Madison
Carolina Mendoza Cavazos
University of Wisconsin–Madison
Laura Knoll (ljknoll@wisc.edu)
University of Wisconsin–Madison

Research Article

Keywords: Cryptosporidium parvum, Toxoplasma gondii, STAg, RNA sequencing, Ileum, Cecum

Posted Date: May 14th, 2021

DOI: https://doi.org/10.21203/rs.3.rs-491899/v1

Dual transcriptomics to determine interferon-gamma independent host response to intestinal *Cryptosporidium parvum* infection.

Gina M. Gallego-Lopez[1,2,τ], Carolina Mendoza Cavazos[2τ], Andrés M. Tibabuzo Perdomo[2], Andrew L. Garfoot[2], Roberta M. O'Connor[3*], Laura J. Knoll[2*]

[1] Morgridge Institute for Research, Madison, WI, 53715, USA

[2] Department of Medical Microbiology and Immunology, University of Wisconsin—Madison, Madison, WI, 53706, USA

[3] Department of Veterinary Microbiology and Pathology, College of Veterinary Medicine, Washington State University, Pullman, WA 99164 USA

τ Both authors contributed equally.

*Corresponding authors

Keywords

Cryptosporidium parvum, *Toxoplasma gondii*, STAg, RNA sequencing, Ileum, Cecum,

Abstract

Background: Protective immune responses to *Cryptosporidium parvum*, a zoonotic, gastrointestinal parasite, are primarily dependent on the presence of interferon-gamma (IFNγ). We discovered that treatment with soluble *T. gondii* antigen (STAg) reduces *Cryptosporidium parvum* shedding in the absence of IFNγ. To identify the protective IFNγ independent responses elicited by STAg, we conducted a transcriptomic analysis of intestinal sections of IFNγ-deleted, *C. parvum* infected or uninfected mice treated with STAg or PBS.

Results: STAg treatment reduced oocyst shedding in *C. parvum* infected IFNγ-deleted mice. Gene ontology analysis of the intestinal transcriptomes suggested that both *C. parvum* infection and STAg treatment changes the transcript abundance of genes involved in the host cell membrane, intracellular and extracellular transport, and immune responses. We found in high abundance 37 genes related to IFN type I response in infected mice treated with STAg. Among these genes, members of the oligoadenylate synthetase and Schlafen family were identified.

Conclusions: STAg treatment of *C. parvum* infected mice induced both host immune and metabolic changes associated with a reduction in shedding. Several components of the type I interferon immune response were more abundant in the ileum of *C. parvum* infected in IFNγ-deleted mice. Future studies will explore the role of type I IFN mediated immune responses in controlling *C. parvum* infections. STAg treatment appears to only affect the host transcriptome while the parasite transcriptome remains unaffected. Several *C. parvum* genes, including mucin genes, are more abundant during the infection of animals, which opens new avenues in *C. parvum* research.

Background:

Cryptosporidium is an enteric, protozoan parasite of global distribution that causes the diarrheal disease, cryptosporidiosis. *C. parvum,* the most studied species of the 31 species of *Cryptosporidium* reported until now*,* can cause severe diarrhea in many species, including calves and humans (1). In human immunodeficiency virus (HIV) infected patients and other immunocompromised individuals, *Cryptosporidium* causes a chronic, debilitating, and sometimes lethal diarrheal disease (2). Additionally, there is an association between *Cryptosporidium* and colorectal cancer (3–6) and recent studies have reported induction of digestive carcinoma in *Cryptosporidium* infected mice (7–9). Because there is neither a vaccine (10,11) nor effective therapeutics (12–14) to prevent and treat cryptosporidiosis in immunocompromised patients, characterization of protective immune responses and identification of new therapeutics are medical and veterinary imperatives.

C. parvum is transmitted via the oral-fecal route by consuming food or water contaminated with oocysts, the environmentally resistant stage of the parasite (15,16). Once inside the host, the oocyst releases sporozoites which invade epithelial cells of the gastrointestinal tract. The parasite undergoes several rounds of asexual replication before moving into sexual replication, all within gut enterocytes. Although the parasite is intracellular it remains extra-cytoplasmic, forming a feeder organelle by which it extracts nutrients from the host cell. Because of its very reduced metabolism, *Cryptosporidium* relies on the host cell for nucleotides (17,18), fatty acids (8,9), and glutaminolysis (21).

The life cycle culminates in the production of oocysts that are released into the environment in the feces (17,22).

During *C. parvum* infection the cytokine interferon-gamma (IFNγ) plays a central role in controlling infection in both innate and cell-mediated immune response (23,24) through a variety of mechanisms. IFNγ inhibits parasite invasion, changes the intracellular iron (Fe^{2+}) concentration in enterocytes that the parasite requires (25), and participates in the clearance of the parasite (24). Patients with IFNγ deficiency are more likely to develop chronic *C. parvum* infection (26). While wild-type mice are resistant to *C. parvum* infection, IFNγ-deficient mice are highly susceptible (23,27,28). Treatment of intact mice with IFNγ neutralizing antibodies renders these mice susceptible to *C. parvum* infection (29). IFNγ also induces up-regulation of the host enzyme indoleamine 2,3-deoxygenase (IDO), inducing tryptophan starvation (30) and killing the parasite. IFNγ is produced by natural killer (NK) cells (31), macrophages (32), and dendritic cells (33) in response to *Cryptosporidium* infection, and all these cell types have a protective role in the IFNγ-dependent innate immune response (34). Also, IFNγ plays a role in *Cryptosporidium* cell-mediated adaptive immune responses, inducing differentiation of naïve CD4 T cells to Th1 cells which secrete more IFNγ, produce IgG2 and promote cytotoxic T cell differentiation (24,29,35–37).

To identify novel *C. parvum* immune responses, we tested a non-infectious extract of soluble *Toxoplasma gondii* antigens (STAg) for efficacy against *C. parvum* infection. STAg was previously found to protect against viral, bacterial, and parasitic infections by

induction of various innate immune responses. In mice infected with the avian influenza virus H5N1, STAg treatment reduced viral titers in the lungs, and induced a strong gamma interferon (IFNγ) response resulting in increased survival (38). STAg treatment was also able to prevent experimental cerebral malaria in mice challenged with *Plasmodium berghei* via induction of IL-12 and IFNγ and subsequent reduction of parasitemia (39). Additionally, STAg treatment provided resistance against *Listeria monocytogenes* bacterial infection by reducing the bacterial burden in the spleen and liver by stimulation of TLR11 and promoting recruitment of Ly6C CCR2+ inflammatory monocytes (40).

Because STAg exhibited immunomodulatory activity protective against a variety of pathogens, for these studies, we tested STAg for anti-cryptosporidial activity. To mimic immunocompromised patients, we used IFNγ-deletion mice to define the IFNγ independent host response to *C. parvum*. Even in the absence of IFNγ, STAg treatment reduced *C. parvum* oocyst shedding, indicating that IFNγ independent immune responses were effective against the parasite. We examined the effect of STAg treatment on host gene expression to identify components of the immune response responsible for alleviating *C. parvum* infection in an IFNγ independent scenario.

Results

STAg treatment reduces the oocyst shedding in *C. parvum* infected IFNγ-deleted mice.

To evaluate if STAg treatment would affect *C. parvum* infection, IFNγ-deleted female mice were infected with $1x10^7$ *C. parvum* oocysts Iowa II strain by oral gavage then treated intraperitoneally with 1 mg STAg or PBS control on 1, 3, and 5 days post-infection (dpi). Fecal samples were collected every other day from 0 to 14 dpi. Oocysts shedding over time was quantified by qPCR (18) and the area under the curve was calculated. We observed that STAg treatment significantly reduced oocyst shedding compared with the PBS treated group ($p=0.030$), indicating that STAg has a therapeutic or immunomodulatory effect against *C. parvum* infection (Fig 1A). The experiment was repeated with IFNγ-deleted mice infected with $1x10^5$ Nano luciferase (Nluc) *C. parvum* oocysts Iowa II strain and oocyst shedding over time was quantified by NLuc expression (42). STAg treatment again significantly reduced the oocyst shedding (Fig 1B; $p=0.034$) confirming our first results (Fig 1A). From these experiments, we concluded that STAg treatment reduces *C. parvum* oocyst shedding in the absence of IFNγ.

Murine intestinal sections were sequenced to determine the interferon-gamma independent transcriptomic response to *C. parvum* infection

To determine the underlying mechanisms by which STAg treatment successfully reduced *C. parvum* shedding in an IFNγ independent manner, we obtained a global view of the transcriptomic changes of the host and parasite elicited by STAg treatment via RNAseq of intestinal tissue. To optimize the collection of intestinal tissue with the highest concentration of parasites, we infected IFNγ-deleted female mice with NLuc *C. parvum* and visualized the parasites throughout the mouse intestinal tract using an in

vivo imaging system (IVIS). Using this technique, Nluc *C. parvum* was localized mainly in the cecum and ileum at 9 dpi (Fig 1C).

To investigate the changes in the transcriptome attributable to STAg in the setting of *C. parvum* infection, mice were infected, treated and samples collected as shown in Fig 2A. Infected mice treated with PBS shed more oocysts than STAg treated infected mice (Fig 2B), indicating that results in this experiment were analogous to experiments shown in Fig 1. As *C. parvum* infects and replicates in enterocytes (15,43,44), we collected the epithelial cell layer in the ileum and caecum for transcriptomic analysis. This methodology allowed us to remove the mucus layer and to concentrate the parasite transcriptome relative to the host transcriptome. RNA was isolated by the Trizol method and libraries prepared for polyA enrichment. Raw reads were processed and analyzed for differential expression and gene ontology enrichment (Fig 2C and Table S1).

Intestinal transcriptomic response to *C. parvum* oral challenge is the most prominent in the host's ileum.

A total of 12 differential gene expression comparisons between tissues, treatments, and infection status were conducted for *Mus musculus* (Table S2) and *C. parvum* (Table S3) transcripts. Principal Component Analysis (PCA) was used to visually compare the ileal and cecal transcriptomes of mice treated with STAg or PBS with and without *C. parvum* infection (Fig 3). Clustering of normalized values calculated by DESeq2 indicates a clear separation between ileal and cecal samples. Ileal samples

from STAg treated animals (n=6, n=3 per infection group), clustered by infection status (Fig 3, right side). One of the ileal samples from the PBS treated infected group does not cluster with the other infected samples, likely due to the percent of reads mapped to the *C. parvum* genome (5.56% vs 1.21 and 1.66%). The cecal samples did not cluster significantly based on infection or treatment.

In terms of the host transcriptomic response to infection and STAg treatment, we observed a low number of differentially expressed genes (DEGs) when comparing the PBS and STAg treatment while maintaining tissue and infection status constant, (Table S2 comparisons 1-4 and Fig 4 A-B). In the ileum, STAg treatment had 13 significant DEGs compared to PBS treatment (Fig 4A). Only a single gene, Myosin Binding Protein C2 (Mybpc2), is shared between comparisons 1 and 2 (Fig S1), highlighting that it is less abundant with STAg treatment with or without infection.

We also compared infection status while maintaining treatment type constant (Table S2 comparisons 5-8 and Fig 4 C-D) and observed the largest number of DEG in these comparisons, which is not surprising as in these comparisons we are capturing the host cell response to infection. Whether STAg or PBS treated, more than 100 genes were significantly differentially expressed within the ileum (Fig 4C) between infected and uninfected animals. Within the STAg treated mice, a total of 129 genes for ileum (Fig 4C) and 78 for the cecum (Fig 4D) were classified as differentially expressed. Out of those 129 genes within the ileum of STAg treated mice, 100 were exclusive to the ileum, and 7 were shared with the cecum of STAg treated mice. The remaining 22

genes were shared with PBS treated, 20 within the ileum and 2 within the cecum (Fig S2). Out of 78 cecal DEGs between infected and uninfected STAg treated mice (Fig 4D), 61 were exclusive to the cecum, 7 were shared with the ileum of STAg treated mice. The remaining 10 genes were not exclusive to STAg treatment and shared with PBS treated groups: 5 ileum PBS and 5 cecum PBS treated groups (Fig S2). Only 2 genes were shared between every single comparison when treatment was maintained constant, and infection status was compared: Keratin 13 (Krt13) and Cytosolic phospholipase A2 gamma (Pla2g4c). Krt13 and Pla2g4c are more abundant in infected mice regardless of treatment status. In the rest of the comparisons, only a low number of transcripts were shared (Fig S1 and S2). PBS treatment allowed us to observe the natural IFNγ independent host responses. Seven genes are exclusive to these control infections (Fig S2, the intersection of comparison 6 and 8).

Overall, the number of DEGs was higher for the ileum (Fig 4A and 4C) than for the cecum (Fig 4B and 4D). These results are not due to unmapped reads, as we observed, on average, ~79% of the reads of both tissues to be uniquely mapped to the host genome. Because the percentage of reads mapped to the *C. parvum* genome is considerably higher in the ileum than the caecum (Fig 3), it is not surprising that this tissue had the highest number of significant DEGs regardless of treatment.

Gene Ontology analysis shows differentially expressed immune response

To further explore the transcriptomic response to *C. parvum* infection and STAg treatment, we used Gene Ontology (GO) enrichment analysis through the Database for

Annotation, Visualization, and Integrated Discovery (DAVID), v6.8 (45,46). Genes that were differentially expressed when treatment was constant and infection was compared (comparisons 5-8 in Table S2) were analyzed for enrichment of three GO term categories: cellular component (Fig S3), molecular function (Fig S4), and biological process (Fig 5). In comparison to the cecum of uninfected STAg treated mice, the cecum of infected STAg treated mice was enriched for cellular component GO terms skewed towards the periphery of the host cells: host membrane (GO:0016020), extracellular space (GO:0005615), and extracellular region (GO:0005576) when comparing infection status (Fig S3). In the ileum of infected-STAg treated mice, as compared to the uninfected-STAg treated mice, DEGs were associated with the mitochondrion (GO: 0005739), the extracellular region (GO:0005576), and the endoplasmic reticulum (GO:0005783) (Fig S3). Cellular component GO-terms had the highest level of enrichment for the cecum samples from STAg treated animals, which was not observed in biological process or molecular function GO terms (Fig S4 and Fig 5). Due to the localization of the parasite on the periphery of the host cell, it is encouraging that we observe GO terms that are related to the extracellular space and cellular trafficking when comparing infection status. We observed major enrichment of molecular function GO terms related to purine metabolism and RNA binding in the ileum of mice infected and STAg treated, which was not observed in the ileum-of mice that were PBS treated (Fig S4).

As expected, the biological process GO terms showed enrichment for host immunity in the ileum of mice treated with STAg (Fig 5). As we tested our hypothesis in IFNγ-

deleted mice, we were expecting signaling that was IFNγ independent. Overall, the innate immune response was significantly associated with type I interferon response, including IFN-alpha signaling (GO:0035457), response to IFN-beta signaling (GO:0035458), downstream targets like defense response to virus (GO:0051607), and response to virus (GO: 0009615) (Fig 5).

Transcript abundance comparisons show immune response and host metabolism changes

As the DEGs in the caecum were highly variable among biological replicates, we focused on ileal samples for further analysis. To compare the abundance of these significant genes across the 6 biological replicates per treatment group, we generated heatmaps charting the normalized reads per animal (Fig 6A and S5). We found 37 genes related to IFN type I in mice infected and treated with STAg (Table 1 and Fig 6A) but not present in mice infected and treated with PBS (Fig S5). Among them were eight oligoadenylate synthetase (OAS) genes, the DDx60 (47), the Dhx58 also known as Lpg2 (48), Mtx2, Tap1, Trim 30a-b-c, the ubiquitin-specific peptidase 18, seven interferon-induced proteins, the Immunity-related GTPase, the immunity-related GTPase family M member 1 and 2; and the Ring finger proteins 213 and 225 (49,50). Similarly, 6 members of the Schlafen gene family (SLFN) were present in higher abundance in STAg treated infected mice versus STAg treated uninfected mice (Comparison 5 and Table 1).

Curiously, 2 transcripts related to gluconeogenesis were identified in lower abundance in the ileum of infected and STAg treated mice when compared to their uninfected counterparts (Fig 6B), Glucose-6-Phosphatase Catalytic Subunit (G6pc), and Fructose 1,6-bisphosphatase (Fbp1). There have been sporadic reports that children (51) or senior individuals (52) with *C. parvum* infection seem to have a lower tolerance for lactose, and we are the first to observe lactase (Lct) transcript to be in lower abundance in infected mice (Fig 6B). In the PBS-treated mice, transcripts for G6pc, Fbp1, and Lct were also less abundant, but they did not achieve the set threshold limits. For Fpp1, the log2 fold change was -1.8 and for Lct, the log2 fold change was -1.9. While G6pc did make the -2 log change cutoff (-2.7), due to variability, G6pc did not meet the padj threshold (p=0.07). These results suggest that infection with *C. parvum* may modulate host carbohydrate metabolism away from gluconeogenesis and disaccharides like lactose. It will be interesting to further investigate if *C. parvum* infection reduces the expression of these enzymes in other hosts or *in vitro* models.

While comparing treatments and keeping infection status constant (Fig 4A), we observed 13 DEGs. STAg treated mice have a lower abundance of Interleukin 10 (IL-10), chemokine 4 (Ccl4), Prostaglandin E Receptor 3 (Ptger3), granzyme B(Gzmb), granzyme K (Gzmk), keratine 14 (Krt14), and others when compared to PBS treatment (Fig 7). These results highlight that STAg treatment reduced the abundance of some inflammatory responses elicited by *C. parvum.*

C. parvum transcript analysis shows no significant differences in gene expression between PBS or STAg treatments

An analysis was conducted to determine if STAg treatment had any effect on the transcriptome of *C. parvum* (Table S3). When a PCA exploration for reads that were aligned to the *C. parvum* genome was conducted, we observed clustering of the ileum, but not the cecum samples (Fig S6). The percentage of uniquely mapped reads to the *C. parvum* genome was significantly lower when compared to host mapping, a result that we were expecting according to other similar studies (53). On average per sample, the ileum had more transcripts that mapped to the *C. parvum* genome than the cecum (Table S1). Differential expression analysis of the parasite transcriptome was performed in the same manner as for the host transcriptome but there were no significant differentially expressed genes between PBS and STAg treated samples. These results indicate that the effect of STAg to lower *C. parvum* oocyst shedding was more likely due to changing the host immune response than a direct effect on the parasite.

The most abundant *C. parvum* transcripts within the ileum, are listed in Tables 2 and 3. The presence of transcripts encoding the *Cryptosporidium* mucin-like glycoproteins (54) such as cpMuc5 (cgd2_430)(55), cpMuc7 (cgd2_450), and cpMuc3 (cgd2_410) were observed in STAg-treated animals (Table 2) and gp40 and the mucin cgd7_4020 in PBS-treated animals (Table 3). For both treatments, the parasite GDP-fucose transporter (CGD3_500) was among the top 10 most abundant transcripts.

Discussion

While nitazoxanide has some efficacy in immune-competent adults, it is not effective in severely immunocompromised patients (56–58) highlighting the need to develop interventions effective in the absence of normal immune responses. To mimic the human immune-compromised state, we used IFNγ-deletion mice to define the IFNγ independent host response to *C. parvum*. Our group and others have determined previously that STAg, through various immune mechanisms, has a protective effect against intracellular infections from multiple pathogens (38–40). In this study, we discovered that STAg treatment also reduced *C. parvum* infection in IFNγ-deleted mice (Fig 1).

Through our transcriptomic analysis, we have found that IFNγ-deleted mice have a higher number of significant DEGs when comparing infection status and maintaining tissue and treatment type constant (Fig 4C and D), suggesting that treatment alone is not sufficient to elicit a host gene expression change. *C. parvum* infection likely acts synergistically with STAg treatment to elicit the type I interferon immune response observed in this transcriptomic study. We suggest this immune response aids in the lower level of parasite shedding detected in the fecal samples of STAg treated mice (Fig 1 and Fig 2B).

Mice that were STAg treated had a total of 207 host DEGs (129 and 78 genes for the ileum and cecum, respectively). Most of the DEGs were of higher transcript abundance within both tissues (87% for ileum and 60% for cecum). Most of the DEGs in the ileum

were classified as belonging to the type I interferon response and its downstream effectors, typically known for their anti-viral activity (Table 1 and Fig 6A). IFNs are a multigenic family of cytokines that regulate different aspects of the immune response. There are three classes of IFN: type I, II, and III, which recognize distinct receptors on cell membranes (59). IFN signaling induces transcription of hundreds of IFN-stimulated genes that further the immune response against viral infection. The IFN type I response is essential in the immune response against viruses (60) but its role in *Cryptosporidium* infection has been poorly characterized. In 2009, Barack *et al*. were the first to describe the IFN type I response to *Cryptosporidium* infection in human and mice enterocytes in vitro (61). Recently, Li *et al*., have shown that upregulation of long-non coding RNAs influences the IFN type I response to *C. parvum* in an in vitro murine model (50). Heo, *et al.,* showed expression of IFN type I genes in lung organoids microinjected with oocysts at 72 hours post-injection (62). Our study is the second *in vivo* transcriptome analysis to report more abundant IFN type I transcripts during *C. parvum* infection.

Among the IFN-stimulated genes, we found in high abundance eight oligoadenylate synthetase (OAS) genes in infected and STAg treated mice (Table 1). OASs synthesize short oligomers that activate RNAse L to cleave cellular and viral RNAs (63,64), participate in apoptosis, and control cellular growth (65). There are at least a dozen OAS proteins in mice and four in humans. OAS-like proteins consist of one OAS domain and two ubiquitin-repeat domains (UBL). Humans have one OAS-like protein, while mice have two OAS-like proteins OASL1 and OASL2. Murine OASL1 has a context-dependent role in the anti-viral response; in the early stages of infection, it forms stress

granules trapping viral RNAs, but in later stages of infection, it downregulates the IFN response (60,63,66).

Among the IFN-stimulated genes, we found six Schlafen gene members (Table 1). The murine Schlafen family has 9 proteins with 5 human homologs. Schlafen proteins have been described to have many potential roles in cell processes, including but not limited to cell differentiation, inhibition of anchorage-independent growth, and regulation of the immune response (67,68). SLFN2 has been shown to regulate type I interferon response via the NF-κβ pathway (69). SLFN3 and its human analog SLFN12 are critical in regulating intestinal epithelial differentiation (43,44). Of this family, the most abundant transcript in our transcriptomic dataset was Schlafen 4 (Slfn4) (70). A previous study has shown in SLFN4 over-expressing mice a reduction in the recruitment of inflammatory macrophages, suggesting SLFN4 as a negative regulator of monocytopoiesis (71). It will be interesting to further explore the relationship between SLFN4 and *C. parvum* infection.

Using GO enrichment analysis, we found an enrichment of immunological terms downstream of IFNα/β signaling (Fig 6). Curiously, no change in IFNα/β transcript abundance was observed. This change in the abundance of the effectors versus the signaling molecules themselves is probably due to the late time point selected. We chose the 9 dpi timepoint to coincide with the peak *C. parvum* oocysts shedding to maximize the number of *C. parvum* transcripts in the datasets. Future experiments will

analyze the IFNα/β signaling pathways throughout the time course of infection to determine the level of protection type I signaling confers against *C. parvum* infection.

STAg treated mice had a lower abundance of IL-10, Ccl4, Ptger3, and granzymes B and K (Fig 7). IL-10 is an anti-inflammatory cytokine, its role is to modulate a balance between pathology and protection against a rampant immune response (72,73). IL-10 is elevated in the stool of *Cryptosporidium* infected Haitian children (72) as well as in patients co-infected with *C. parvum* and HIV (74). In animal models, IL-10 knockout mice are more resistant to *C. parvum* infection (75), but anti-IL-10 antibody treatment in calves does not reduce *C. parvum* shedding (76). Ccl4 is a chemokine independent of IFNγ, whose expression level increases during *C. parvum* infection when compared to control mice (33). A high level of prostaglandins has been observed in *C. parvum* infection, implicated in increased mucosal activity and downregulation of inflammatory cytokine production (77,78). Granzymes induced by NK cells or CD8+ cytotoxic T cells (79) have been found in high abundance in mice and humans infected with *Cryptosporidium*, inducing cell death and cytolysis of infected epithelial cells. They are also associated with apoptosis and colon lesions in AIDS patients co-infected with *Cryptosporidium* (80–83).

Even though we could not assess *C. parvum* differential expression, we report the most abundant *C. parvum* transcripts within the ileum. Among those transcripts, we found the GDP-fucose transporter (CGD3_500) to be abundant in our infected animals, regardless of treatment. In other apicomplexan parasites like *Toxoplasma gondii,* O-fucosylated

glycoproteins can form assemblies that are associated with nuclear pore complexes (84). For both *T. gondii* and *Plasmodium falciparum,* O-fucosylation of thrombospondin-like repeats is required for processing proteins relevant to host cell invasion (85,86). We also found transcripts in high abundance of parasite mucins. Mucins are glycoproteins that have an amino acid composition consisting of 20 to 55% serine, threonine, and proline residues, with extensive chains of O-linked carbohydrates (54) forming homo-oligomers. Mucins have been reported both in the host and in some gastrointestinal parasites. *Cryptosporidium's* mucins are important for attachment and invasion to the host cell (54) or evasion of the host immune system (87). Many essential *Cryptosporidium* proteins are mucin-like proteins such as gp40/15 (88), cpClec, gp30, and gp900 (89). There is a genetic locus of seven mucins denominated cpMuc1-7, which suggests that these seven mucins are regulated and expressed in a coordinated fashion with a role in the same biological processes (54). C*ryptosporidium* mucins have high polymorphism between species and genotypes, which suggests gene products might be important virulence determinants subject to immune pressure (54). Recently, it has been published that mucins play a role in tissue tropism between gastric and intestinal *Cryptosporidium* species and also determine differences in host range among *Cryptosporidium* species (90,91). Further investigation is required for the validation of the differential expression of *C. parvum* transcriptomic response to STAg treatment.

Conclusions

Our results show that STAg treatment reduces the oocyst shedding in *C. parvum* infected IFNγ-deleted mice. We evaluated the effect of STAg treatment on both the

mouse and in the parasite transcriptomes. The detailed analysis of the transcriptome suggests that STAg treatment induces both host inflammatory responses and metabolism changes relevant to gluconeogenesis and disaccharide breakdown. Particularly notable is the induced type I interferon immune response in the ileum of *C. parvum* infected in IFNγ-deleted mice. We hypothesize that this immune response can lower the level of parasites shed in the fecal samples of STAg treated mice, but further experiments are needed to confirm this observation.

In terms of the parasite transcriptomic regulation, we did not find significant differences in transcript abundances when comparing STAg vs PBS treatment. It is possible that STAg treatment only affects the host transcriptome while the parasite transcriptome remains unaffected. This lack of differential *C. parvum* expression could also be due to the limitations of coverage and sequence depth of our study. While several of the *C. parvum* transcripts were more abundant in the ileum than the cecum, there was also significantly higher mapping of *C. parvum* reads to the ileum. Thus, we focused on the most abundant transcripts within the ileum with both treatments in hopes that the *C. parvum* community can use this *in vivo* data for comparisons with *in vitro* systems. By discovering *C. parvum* genes that are more abundant during infection of animals that lack IFNγ signaling, we are discovering targets that could serve as an alternative route to control infection. A significant addition to the field that opens new avenues in *C. parvum* disease halting research.

List of figures

Figure 1. **Infection time course of *C. parvum* infected mice treated with STAg or PBS. (A).** The area under the curve of treated mice in experiment #1 over 15 days of infection; *p=0.03, Oocyst shedding calculated by qPCR, as described in the methods section. **(B).** The area under the curve of treated mice in experiment #2 over 15 days of infection; *p=0.034, Oocyst shedding calculated by expression of nanoLuciferase, as described in the methods section. **(C)** Bioluminescent imaging of *C. parvum* in mice small intestine: the small intestine of mice infected 9 dpi with Nluc *C. parvum* Iowa II strain at $1x10^5$ showing a higher abundance in the ileum and cecum regions. Radiance scale bar (p/sec/cm^2/s).

Figure 2. Mice Experimental Design and analysis for RNA sequencing. **(A).** For the RNAseq analysis, 12 mice, 6 infected and 6 non-infected were treated with PBS or STAg. The treatment was administered 4 hours prior to infection ($2.5x10^5$ Nluc *C. parvum* Iowa II strain oocyst by oral gavage) and 1, 3, and 5 days post-infection. Fecal samples were collected every other day and infection quantified by nanoLuciferase expression. Mice were euthanized on 9 dpi and ileum and cecum samples were collected. **(B).** Oocyst shedding calculated by expression of nanoLuciferase, as described in the methods section, and area under the curve calculated over 9 dpi. Each square (PBS) or each triangle (STAg) represents a mouse. Statistic differences were analyzed by t-test using GraphPad PRISM and the mean of each group is represented

with a line. **(C).** RNA sequencing analysis flowchart listing the programs and packages utilized for reading and analysis. Versions used are indicated in parenthesis.

Figure 3. Principal Component Analysis (PCA) of ileum and cecum samples. PCA plot from normalized values calculated by DESeq2. Mapping of the cecum and ileum intestinal section to *Mus musculus* genome. Symbol filling represents *C. parvum* infection status: Uninfected (open); Infected (filled). Symbol color represents treatment: control treatment PBS (blue); Soluble *T. gondii* antigen, STAg (red). The text above individual mice corresponds to the percent of reads uniquely mapped to the *C. parvum* genome.

Figure 4. Host Differential expressed genes by treatment, infectious status, and tissue. (A). Host genes with significantly different abundance when infection status was constant, and treatment was compared in the ileum (comparisons 1 and 2) and **(B)** cecum (comparisons 3 and 4). **(C).** Host genes with significantly different abundance when treatment was constant and infection status was compared in the ileum (comparisons 5 and 6) and **(D)** cecum (comparison 7 and 8). Significant calls had a < 0.05 padj value and a > 2 absolute log2fold change. Shared sets of significant calls are represented by overlapping regions in the diagram. Color scale represents a higher number of calls as darker shades of grey. The specifics of each mouse group can be found in the table (Tables S2 and S3). Visualization of all possible comparisons can be found in Figure S1 and Figure S2.

Figure 5. Host gene ontology (GO) of biological process (BP) in STAg and PBS treated mice. Differentially expressed genes (DEGs) in comparisons 5-8 were analyzed for gene ontology enrichment of biological process (BP)**,** using the Database for Annotation, Visualization, and Integrated Discovery (DAVID, v6.8). Only GO terms populated by 3 or more DEGs were included in these visualizations ($p < 0.05$). Bar filling color represents treatment: control treatment PBS (blue); Soluble T. gondii antigen, STAg (red).

Figure 6: Heatmap of differentially expressed genes in the ileum of mice treated with STAg (comparison 5). The top 25 more **(A)** and less **(B)** abundant transcripts (ranked by log2 fold change). Each column represents a biological replicate.

Figure 7: Heatmap of differentially expressed genes in the ileum of infected mice treated with STAg or PBS. 13 genes (ranked by log2 fold change) were found to be differentially expressed in the ileum between infected mice treated with PBS or STAg. Each column represents a biological replicate.

Supplementary Material:

Table S1: Percent of uniquely mapped reads per genome**.**

Table S2. Host all possible comparisons between tissue, treatment, and infection status.

Table S3. *C. parvum* all possible comparisons between tissue, treatment, and infection status.

Figure S1. Host differentially expressed genes by all possible comparisons when the infectious status is constant. Color scale represents a higher number of calls as darker shades of grey.

Figure S2. Host differentially expressed genes by all possible comparisons with treatment held constant. Color scale represents a higher number of calls as darker shades of grey.

Figure S3. Host gene ontology (GO) of cellular component (CC)) in STAg and PBS treated mice. Differentially expressed genes (DEGs) in comparisons 1-2 and 3-5 were analyzed for gene ontology enrichment of cellular component (CC) using the Database for Annotation, Visualization, and Integrated Discovery (DAVID, v6.8). Only GO terms populated by 3 or more DEGs were included in these visualizations ($p < 0.05$). Bar filling color represents treatment: control treatment PBS (blue); Soluble T. gondii antigen, STAg (red).

Figure S4. Host gene ontology (GO) of molecular function (MF) in STAg and PBS treated mice. Differentially expressed genes (DEGs) in comparisons 1-2 and 3-5 were used for gene ontology enrichment of molecular function (MF) using the Database for Annotation, Visualization, and Integrated Discovery (DAVID, v6.8). Only GO terms

populated by 3 or more DEGs were included in these visualizations ($p < 0.05$). Bar filling color represents treatment: control treatment PBS (blue); Soluble T. gondii antigen, STAg (red).

Figure S5. Heatmap of host differentially expressed genes in the ileum of mice treated with PBS (A) The top 25 more and **(B)** less abundant transcripts in ileum treated with PBS; The color scale was determined by log2 fold change in Infected and non-infected mice. Each column represents a biological replicate.

Figure S6: Principal Component Analysis (PCA) of mapping of ileum and cecum samples to the *C. parvum* genome. PCA plot from normalized values calculated by DESeq2. Symbol filling represents host tissue: ileum (open); cecum (filled). Symbol color represents treatment: control treatment PBS (blue); Soluble *T. gondii* antigen, STAg (red)**.**

Supplemental file 1

Supplemental file 2

Supplemental file 3

Supplemental file 4

Supplemental file 4

Supplemental file 5

Supplemental file 6

Supplemental file 7

Supplemental file 8

Supplemental file 9

Supplemental file 10

Supplemental file 11

Supplemental file 12

Methods

Cryptosporidium parvum: nanoLuciferase (Nluc) *C. parvum* oocysts (Iowa II Strain) were purchased from the University of Arizona.

STAg preparation: The STAg was prepared as described originally (92) except for the following changes. ME49 *T. gondii* parasites were grown in HFFs under mycoplasma-free standard cell culture conditions in Dulbecco's modified Eagle medium (DMEM) supplemented with 10% fetal bovine serum, 1% penicillin-streptomycin, and 2 mM L-glutamine. When the parasites were beginning to lyse the host cells, monolayers were scraped, passed twice through a 27-gauge needle, and pelleted at 500 g. Parasites were washed in phosphate-buffered saline (PBS) without divalent cations and resuspended to 4 x 10^8 parasites per mL. After sonication with five 30-s pulses, parasites were centrifuged at 100,000 g for 45 min and supernatants were collected and stored at 80°C until use.

Mouse Infections

Experiment 1: Eight 4-week-old females were infected by oral gavage with $1x10^7$ *C. parvum* Iowa II oocysts and given STAg (1 mg/dose via ip injection,) or PBS (4 mice per treatment group) at 1, 3, and 5 dpi. Fecal samples were collected every other day from day 0-day 14 and oocyst shedding was quantified by qPCR following the protocol previously published (41). Shedding overtime was graphed and the area under the curve was calculated for each mouse. The area under the curve was averaged for each group and compared by t-test two-tailed using GraphPad PRISM.

Experiment 2: Sixteen, 4-week-old C57BL/6 IFNγ-deleted mice (B6.129S7-Ifngtm1Ts/J, Jackson Laboratories; 8 females and 8 males) were infected by oral gavage with $1x10^5$ Nluc *C. parvum* oocysts (Iowa II Strain). 4 males and 4 females received STAg and the other 4 males and 4 females received PBS (1 mg/dose via ip injection) at 1, 3, and 5 dpi. Fecal samples were collected every other day from day 0-day 14 and oocyst shedding quantified by nanoLuciferase expression following the protocol previously published (42). Shedding overtime was graphed and the area under the curve was calculated for each mouse. Area under the curve was averaged for each group and compared by t-test (two-tailed) using GraphPad PRISM.

Experiment 3: Twelve 4-week-old females C57BL/6 IFNγ-deficient mice (B6.129S7-Ifngtm1Ts/J, Jackson Laboratories) were placed into 4 groups: Uninfected-PBS, Uninfected-STAg, Infected-PBS, Infected-STAg. All mice received pre-treatment with STAg or PBS 4 hours before infection. Then, 2.5 $x10^5$ nanoLuciferase Iowa II strain

oocyst/mice were given by oral gavage to the infected groups. At 24, 48, and 72 hours post-infection, the mice were treated with either STAg or PBS. From 6 to 9 dpi, the mice were weighed, and individual fecal samples were collected to evaluate infection levels. On 9 dpi, mice were euthanized. The intestine was isolated and rinsed using a gavage needle and scrapped using a single-use sterile cell scrapper with sterile 1X PBS. A section of 2 cm of ileum from each mouse was processed. Similarly, the cecum was isolated and rinsed to remove its content. The cecum bag was opened and scraped. Scrapping was performed to isolate the epithelial layer. After microscopic verification, the material was resuspended in 1 mL of 1X Hanks Balanced Salt Solution- HBSS (Corning). After centrifugation, the pellet was resuspended in 1 mL of Trizol (Ambion), vortexed, and saved at -80°C.

Generation of RNA and RNA Sequencing: We used the University of Wisconsin – Madison Biotechnology Center's Gene Expression Center Core Facility (Research Resource Identifier - RRID:SCR_017757) for RNA isolation, RNA library preparation, and the DNA Sequencing Facility (RRID:SCR_017759) for sequencing and demultiplexing of reads. Libraries were prepared for polyA enrichment (Illumina TruSeq Stranded mRNA). Samples were run in duplicate in two lanes of a 2x100bp S1 Flowcell (Novaseq6000). On average a total of 41.5 million reads (min: 36 million, max: 49.6 million) paired-end 150-bp reads per sample were generated. The quality of the reads was determined (FastQC v0.11.9 (93), a threshold of 34 was selected, and only reads that met the threshold were used for further analysis.

Transcriptome assembly and Differential expression Analysis: We trimmed the data to remove low-quality reads (Trimmomatic, v0.39) (6) Mapping reads to two genomes: *Mus musculus* strain C57BL/6 (GRCm38.p6, release38; NCBI) and *Cryptosporidium parvum* (Iowa II, release 49; CryptoDB) was conducted (Spliced Transcripts Alignment to a Reference program, v2.7.5c) (95,96). Default parameters were selected with the following exceptions: maximum mismatch (2-bps), minimum intro length (20-bps), and maximum intron length (100000-bps). Quantification of mapped reads and the generation of a counts table were conducted (RSEM v1.3.1(97). Counts were imported into R (tximport v1.16) (98), and differential expression analysis was conducted (DESEq2 v1.28.1) (99). The log-transformed DESeq2 values were used for the generation of PCA plots. For reads mapped to the host genome, we selected the following thresholds: false discovery rate (10%), adjusted p-value (< 0.05), and an absolute log2fold change (>2). If a differential expression call met those parameters, we called that gene differentially expressed. (Supplemental CSV file 1-12). Given that the average *C. parvum* percentage mapping (ileum= 2.58% and cecum= 0.33%) was significantly lower than the host mapping (ileum= 78.92% and cecum= 77.95%), we selected only two thresholds to call for *C. parvum* significance: false discovery rate (10%), and adjusted p-value (< 0.05). Lists of significant genes were used as input for gene ontology enrichment analysis using the Database for Annotation, Visualization, and Integrated Discovery (DAVID, v6.8 (45,46) for visualization of this enrichment only terms were populated by 3 or more genes were charted ($p < 0.05$).

Luciferase assay: Mouse infections were confirmed by luciferase measurement of mouse fecal samples following a protocol previously reported (42). Briefly, 20mg of fecal sample was weighed into a 1.5-ml microcentrifuge tube and homogenized in 1mL of lysis buffer (50mM Tris-HCl, 10% glycerol, 1% Triton-X, 2mM dithiothreitol (DTT), 2mM EDTA) using 10–15 glass beads (3mm) and a vortex mixer for 1 min, followed by clarification of lysate by brief centrifugation. One hundred microliters of lysate were mixed with an equal volume of NanoGlo Luciferase Buffer, prepared with 1:50 dilution of the substrate (Promega, corporation). Three technical replicates per sample were conducted. Luminescence was measured in a synergy HT luminator (BioTek).

Oocyst purification from mouse feces: Oocysts were purified from mouse fecal samples using sucrose suspension followed by a cesium chloride (CsCl) centrifugation as previously published (42). Mouse feces were suspended in water, homogenized, and passed through two filters. This filtered suspension was mixed 1:1 with aqueous sucrose solution (specific gravity 1.33) and centrifuged at 1,000g for 5 min. Oocysts were collected from the supernatant and suspended in 0.85% NaCl saline solution. Then, 0.5 mL of this preparation was overlaid onto 0.8 ml of 1.15 specific gravity CsCl and centrifuged for 3 min at 16,000g. Oocysts were collected from the top mL of the sample, washed in 0.85% saline, and resuspended in 1x penicillin-streptomycin antibiotic solution.

Quantification of oocysts by immunofluorescence: Samples were diluted in PBS, fixed with methanol on the well of a glass slide, and incubated with Crypt-a-Glo antibody

(Waterborne INC) for 30 minutes at 37° C. The slide was then gently washed with 1X PBS and allowed to dry. A drop of antifade mounting media with DAPI-counterstain (Vectashield) and a coverslip were added. The total number of oocyst/well was quantified at 40x by microscopy with a Zeiss Axioplan III equipped with a triple-pass (DAPI/fluorescein isothiocyanate [FITC]/Texas Red) emission cube, differential interference contrast optics, and a monochromatic Axiocam camera operated by Zen software (Zeiss). Oocysts / µL were calculated as an average of at least three microscopic readings.

Bioluminescent imaging of *C. parvum* in mice small intestine by In vivo Imaging System (IVIS): Female IFNγ-deleted mice (n=5) were infected with $1.5x10^5$ Nluc Iowa II strain *C. parvum* oocysts via oral gavage. Mice were euthanized 9 dpi, their small intestines removed, cleaned, and temporarily stored in PBS to avoid drying of the sample. Prior to imaging, the PBS was removed and each sample was transferred to a clean petri dish containing the luciferase activity buffer (NanoGlo®, Promega). The sample was incubated in the buffer for 2 minutes and transferred to an IVIS to collect bioluminescence data for an exposure time of 5 minutes.

List of abbreviations

IFNγ = Interferon gamma; Nluc = Nano luciferase; STAg= soluble Toxoplasma gondii Antigen; RNA= ribonucleic Acid; PolyA= poly adenylation; DEGs= differential expressed genes; OAS= oligoadenylate synthetase; C. parvum= Cryptosporidium parvum; qPCR = quantitative Polymerase chain reaction; IVIS = *in vivo* imaging system; AUC = are

under the curve; DPI: Days post-infection; GO: Gene ontology; PBS: Phosphate buffered saline; PCA: Principal component analysis; RNAseq: High-throughput RNA sequencing; STAR: Spliced Transcripts Alignment to a Reference program; SLFN = Schlafen gene family ; ATP = adenosin Triphosphate; padj = P value adjusted. DAVID = Database for Annotation, Visualization, and Integrated Discovery. FDR = false discovery rate; CC = Go term integral component of membrane; MF = Go Term Molecular Function; BP= Go Term Biological Process

Declarations

Availability of data and materials

All of the data is available. All raw RNA sequencing data have been deposited in the NCBI Sequence Read Archive: http://www.ncbi.nlm.nih.gov/bioproject/726295

SubmissionID: SUB9557041

BioProject ID: PRJNA726295

RNA sequencing data have been supplied for public availability to HostDB.org and CryptoDB.org. Differential expression analysis output and counts of mapped reads per individual biological replicate are available (Supplemental files 1-12).

Ethics approval

All animal studies were carried out in compliance with the Animal Research: Reporting of In Vivo Experiments (ARRIVE) guidelines and approved by the Institutional Animal Care and Use Committee (IACUC) of the University of Wisconsin School of Medicine

and Public Health. The University of Wisconsin is accredited by the International Association for Assessment and Accreditation of Laboratory Animal Care. All methods and all experimental protocols were approved by the University of Wisconsin IACUC (protocol M005217) as well as the Office of Biological Safety (protocol B00000086).

Consent for publication: Not applicable.

Consent to participate: Not applicable.

Competing interests: We confirm that none of the authors have any competing interests in accordance with BioMed Central's guidelines.

Funding: This work was funded by the National Institutes of Health (R21AI122898 RMO, LJK; R01AI144016 LJK; T32007215 CMC), SciMed Graduate Research Scholars Fellowship UW-Madison (CMC), Foster Wisconsin Distinguished Fellowship from the Food and Research Institute (CMC), The Hartwell Foundation postdoctoral fellowship (ALG), and Morgridge Postdoctoral Fellowship supported by the Morgridge Institute for Research (GMGL). Funding bodies had no role in the design of the study and collection, analysis, and interpretation of data and in writing the manuscript.

Authors' contributions: Design of experiments: GMGL, RMO & LJK. Conceptualization: RMO & LJK; RNA sequencing processing: CMC; Funding

acquisition: RMO & LJK; Investigation: GMGL, CMC, AMTP; Methodology: GMGL, CMC, ALG, AMTP; Project administration: LJK. Resources: RMO & LJK; Supervision: LJK. Visualization: GMGL, CMC, AMTP; Writing: GMGL CMC; Writing – review & editing: CMC, ALG, AMTP, RMO and LJK. All authors read and approved the final manuscript.

Acknowledgments: We sincerely thank Bruno Martorelli Di Genova, Patrick Cervantes, and Carlos J. Ramirez for their lab assistance with IVIS and mice work.

References

1. Casemore DP. Epidemiological aspects of human cryptosporidiosis. Epidemiol Infect [Internet]. 1990 Feb 15;104(1):1–28. Available from: https://www.cambridge.org/core/product/identifier/S0950268800054480/type/journal_article
2. Cabada MM, White AC. Treatment of cryptosporidiosis: do we know what we think we know? Curr Opin Infect Dis [Internet]. 2010/08/07. 2010 Oct;23(5):494–9. Available from: http://www.ncbi.nlm.nih.gov/entrez/query.fcgi?cmd=Retrieve&db=PubMed&dopt=Citation&list_uids=20689422
3. Sulżyc-Bielicka V, Kuźna-Grygiel W, Kołodziejczyk L, Bielicki D, Kładny J, Stępień-Korzonek M, et al. Cryptosporidiosis in Patients with Colorectal Cancer. J

Parasitol [Internet]. 2007 Jun;93(3):722–4. Available from: http://www.bioone.org/doi/abs/10.1645/GE-1025R1.1

4. Osman M, Benamrouz S, Guyot K, Baydoun M, Frealle E, Chabe M, et al. High association of Cryptosporidium spp. infection with colon adenocarcinoma in Lebanese patients. Chamaillard M, editor. PLoS One [Internet]. 2017 Dec 19;12(12):e0189422. Available from: http://dx.doi.org/10.1371/journal.pone.0189422

5. Zhang N, Yu X, Zhang H, Cui L, Li X, Zhang X, et al. Prevalence and Genotyping of Cryptosporidium parvum in Gastrointestinal Cancer Patients. J Cancer [Internet]. 2020;11(11):3334–9. Available from: http://www.jcancer.org/v11p3334.htm

6. Shebl FM, Engels EA, Goedert JJ. Opportunistic Intestinal Infections and Risk of Colorectal Cancer Among People with AIDS. AIDS Res Hum Retroviruses [Internet]. 2012 Sep;28(9):994–9. Available from: http://www.liebertpub.com/doi/10.1089/aid.2011.0185

7. Certad G, Ngouanesavanh T, Guyot K, Gantois N, Chassat T, Mouray A, et al. Cryptosporidium parvum, a potential cause of colic adenocarcinoma. Infect Agent Cancer [Internet]. 2007 Dec 21;2(1):22. Available from: https://infectagentscancer.biomedcentral.com/articles/10.1186/1750-9378-2-22

8. Pinon A, Dei-Cas E, Delhaes L, Chassat T, Creusy C, Guyot K, et al. Development of Cryptosporidium parvum-Induced Gastrointestinal Neoplasia in Severe Combined Immunodeficiency (SCID) Mice: Severity of Lesions Is Correlated with Infection Intensity. Am J Trop Med Hyg [Internet]. 2010 Feb

1;82(2):257–65. Available from: http://www.ajtmh.org/content/journals/10.4269/ajtmh.2010.09-0309

9. Certad G, Benamrouz S, Guyot K, Mouray A, Chassat T, Flament N, et al. Fulminant Cryptosporidiosis after Near-Drowning: a Human Cryptosporidium parvum Strain Implicated in Invasive Gastrointestinal Adenocarcinoma and Cholangiocarcinoma in an Experimental Model. Appl Environ Microbiol [Internet]. 2012 Mar 15;78(6):1746–51. Available from: http://aem.asm.org/lookup/doi/10.1128/AEM.06457-11

10. Checkley W, White AC, Jaganath D, Arrowood MJ, Chalmers RM, Chen X-M, et al. A review of the global burden, novel diagnostics, therapeutics, and vaccine targets for cryptosporidium. Lancet Infect Dis [Internet]. 2014/09/29. 2015 Jan;15(1):85–94. Available from: https://www.ncbi.nlm.nih.gov/pubmed/25278220

11. Innes EA, Bartley PM, Rocchi M, Benavidas-Silvan J, Burrells A, Hotchkiss E, et al. Developing vaccines to control protozoan parasites in ruminants: Dead or alive? Vet Parasitol [Internet]. 2011 Aug;180(1–2):155–63. Available from: https://linkinghub.elsevier.com/retrieve/pii/S030440171100389X

12. Squire SA, Ryan U. Cryptosporidium and Giardia in Africa: current and future challenges. Parasit Vectors [Internet]. 2017 Apr 20;10(1):195. Available from: http://www.ncbi.nlm.nih.gov/pubmed/28427454

13. Desai AN. Cryptosporidiosis. JAMA [Internet]. 2020;323(3):288. Available from: http://www.ncbi.nlm.nih.gov/pubmed/31961421

14. Widmer G, Carmena D, Kváč M, Chalmers RM, Kissinger JC, Xiao L, et al.

Update on Cryptosporidium spp.: highlights from the Seventh International Giardia and Cryptosporidium Conference. Parasite [Internet]. 2020 Mar 13;27(14):14. Available from: http://www.ncbi.nlm.nih.gov/pubmed/32788035

15. Tzipori S, Widmer G. A hundred-year retrospective on cryptosporidiosis. Bone. 2011;23(1):1–7.

16. Shahiduzzaman M, Daugschies A. Therapy and prevention of cryptosporidiosis in animals. Vet Parasitol [Internet]. 2012 Sep;188(3–4):203–14. Available from: http://dx.doi.org/10.1016/j.vetpar.2012.03.052

17. Sateriale A, Striepen B. Beg, Borrow and Steal: Three Aspects of Horizontal Gene Transfer in the Protozoan Parasite, Cryptosporidium parvum. Knoll LJ, editor. PLOS Pathog [Internet]. 2016 Mar 3;12(3):e1005429. Available from: http://www.ncbi.nlm.nih.gov/pubmed/26938451

18. Pawlowic MC, Somepalli M, Sateriale A, Herbert GT, Gibson AR, Cuny GD, et al. Genetic ablation of purine salvage in Cryptosporidium parvum reveals nucleotide uptake from the host cell. Proc Natl Acad Sci U S A [Internet]. 2019;116(42):21160–5. Available from: http://www.ncbi.nlm.nih.gov/pubmed/31570573

19. Zhu G. Current Progress in the Fatty Acid Metabolism in Cryptosporidium parvum. J Eukaryot Microbiol [Internet]. 2003 Jan;51(4):381–8. Available from: http://doi.wiley.com/10.1111/j.1550-7408.2003.tb00098.x

20. Rider SD, Zhu G. Cryptosporidium: genomic and biochemical features. Exp Parasitol [Internet]. 2010 Jan;124(1):2–9. Available from:

http://dx.doi.org/10.1016/j.exppara.2008.12.014

21. Vélez J, Velasquez Z, Silva LMR, Gärtner U, Failing K, Daugschies A, et al. Metabolic Signatures of Cryptosporidium parvum-Infected HCT-8 Cells and Impact of Selected Metabolic Inhibitors on C. parvum Infection under Physioxia and Hyperoxia. Biology (Basel) [Internet]. 2021 Jan 15;10(1):60. Available from: https://www.mdpi.com/2079-7737/10/1/60

22. Laurent F, McCole D, Eckmann L, Kagnoff MF. Pathogenesis of Cryptosporidium parvum infection. Microbes Infect [Internet]. 1999 Feb;1(2):141–8. Available from: https://linkinghub.elsevier.com/retrieve/pii/S1286457999800057

23. You X, Mead JR. Characterization of experimental Cryptosporidium parvum infection in IFN-gamma knockout mice. Parasitology [Internet]. 1998 Dec;117 (Pt 6(1998):525–31. Available from: http://www.ncbi.nlm.nih.gov/pubmed/9881376

24. Chen W, Harp JA, Harmsen AG. Requirements for CD4+ cells and gamma interferon in resolution of established Cryptosporidium parvum infection in mice. Infect Immun [Internet]. 1993 Sep;61(9):3928–32. Available from: http://www.ncbi.nlm.nih.gov/pubmed/8103040

25. Pollok RCG, Farthing MJG, Bajaj-Elliott M, Sanderson IR, McDonald V. Interferon gamma induces enterocyte resistance against infection by the intracellular pathogen Cryptosporidium parvum. Gastroenterology [Internet]. 2001 Jan;120(1):99–107. Available from: http://www.ncbi.nlm.nih.gov/pubmed/11208718

26. Gomez Morales MA, Ausiello CM, Guarino A, Urbani F, Spagnuolo MI, Pignata C,

et al. Severe, protracted intestinal cryptosporidiosis associated with interferon gamma deficiency: pediatric case report. Clin Infect Dis [Internet]. 1996 May;22(5):848–50. Available from: http://www.ncbi.nlm.nih.gov/pubmed/8722945

27. Griffiths JK, Theodos C, Paris M, Tzipori S. The gamma interferon gene knockout mouse: a highly sensitive model for evaluation of therapeutic agents against Cryptosporidium parvum. J Clin Microbiol [Internet]. 1998 Sep;36(9):2503–8. Available from: https://www.ncbi.nlm.nih.gov/pubmed/9705383

28. Mead JR, You X. Susceptibility differences to Cryptosporidium parvum infection in two strains of gamma interferon knockout mice. J Parasitol. 1998;84(5):1045–8.

29. Leav BA, Yoshida M, Rogers K, Cohen S, Godiwala N, Blumberg RS, et al. An Early Intestinal Mucosal Source of Gamma Interferon Is Associated with Resistance to and Control of Cryptosporidium parvum Infection in Mice. Infect Immun [Internet]. 2005 Dec;73(12):8425–8. Available from: https://www.ncbi.nlm.nih.gov/pubmed/16299343

30. Taylor MW, Feng GS. Relationship between interferon-gamma, indoleamine 2,3-dioxygenase, and tryptophan catabolism. FASEB J [Internet]. 1991 Aug;5(11):2516–22. Available from: http://www.ncbi.nlm.nih.gov/pubmed/1907934

31. Barakat FM, McDonald V, Di Santo JP, Korbel DS. Roles for NK cells and an NK cell-independent source of intestinal gamma interferon for innate immunity to Cryptosporidium parvum infection. Infect Immun [Internet]. 2009 Nov;77(11):5044–9. Available from: http://www.ncbi.nlm.nih.gov/pubmed/19687195

32. Choudhry N, Petry F, van Rooijen N, McDonald V. A protective role for interleukin 18 in interferon γ-mediated innate immunity to Cryptosporidium parvum that is independent of natural killer cells. J Infect Dis [Internet]. 2012 Jul 1;206(1):117–24. Available from: http://www.ncbi.nlm.nih.gov/pubmed/22517912

33. Lantier L, Lacroix-Lamandé S, Potiron L, Metton C, Drouet F, Guesdon W, et al. Intestinal CD103+ dendritic cells are key players in the innate immune control of Cryptosporidium parvum infection in neonatal mice. PLoS Pathog [Internet]. 2013;9(12):e1003801. Available from: http://www.ncbi.nlm.nih.gov/pubmed/24367259

34. McDonald V, Korbel DS, Barakat FM, Choudhry N, Petry F. Innate immune responses against Cryptosporidium parvum infection. Parasite Immunol [Internet]. 2013 Feb;35(2):55–64. Available from: http://www.ncbi.nlm.nih.gov/pubmed/23173616

35. Lean I-S, McDonald V, Pollok RCG. The role of cytokines in the pathogenesis of Cryptosporidium infection. Curr Opin Infect Dis [Internet]. 2002 Jun;15(3):229–34. Available from: http://journals.lww.com/00005176-199808000-00035

36. Aguirre SA, Perryman LE, Davis WC, McGuire TC. IL-4 protects adult C57BL/6 mice from prolonged Cryptosporidium parvum infection: analysis of CD4+alpha beta+IFN-gamma+ and CD4+alpha beta+IL-4+ lymphocytes in gut-associated lymphoid tissue during resolution of infection. J Immunol [Internet]. 1998 Aug 15;161(4):1891–900. Available from: http://www.ncbi.nlm.nih.gov/pubmed/9712058

37. Lemieux M, Sonzogni-Desautels K, Ndao M. Lessons Learned from Protective

Immune Responses to Optimize Vaccines against Cryptosporidiosis. Pathogens [Internet]. 2017 Dec 24;7(1):2. Available from: http://www.mdpi.com/2076-0817/7/1/2

38. O'Brien KB, Schultz-Cherry S, Knoll LJ. Parasite-Mediated Upregulation of NK Cell-Derived Gamma Interferon Protects against Severe Highly Pathogenic H5N1 Influenza Virus Infection. J Virol. 2011;85(17):8680–8.

39. Settles EW, Moser LA, Harris TH, Knoll LJ. Toxoplasma gondii upregulates interleukin-12 to prevent Plasmodium berghei-induced experimental cerebral malaria. Infect Immun. 2014;82(3):1343–53.

40. Neal LM, Knoll LJ. Toxoplasma gondii Profilin Promotes Recruitment of Ly6Chi CCR2+ Inflammatory Monocytes That Can Confer Resistance to Bacterial Infection. PLoS Pathog. 2014;10(6).

41. Godiwala NT, Vandewalle A, Ward HD, Leav BA. Quantification of In Vitro and In Vivo Cryptosporidium parvum Infection by Using Real-Time PCR. Appl Environ Microbiol [Internet]. 2006 Jun;72(6):4484–8. Available from: https://aem.asm.org/content/72/6/4484

42. Vinayak S, Pawlowic MC, Sateriale A, Brooks CF, Studstill CJ, Bar-Peled Y, et al. Genetic modification of the diarrhoeal pathogen Cryptosporidium parvum. Nature [Internet]. 2015 Jul 15;523(7561):477–80. Available from: http://www.nature.com/articles/nature14651

43. Laurent F, Lacroix-Lamandé S. Innate immune responses play a key role in controlling infection of the intestinal epithelium by Cryptosporidium. Int J Parasitol

[Internet]. 2017/09/08. 2017 Oct;47(12):711–21. Available from: https://www.ncbi.nlm.nih.gov/pubmed/28893638

44. Leitch GJ, He Q. Cryptosporidiosis-an overview. J Biomed Res [Internet]. 2012 Jan;25(1):1–16. Available from: http://www.ncbi.nlm.nih.gov/pubmed/3368497

45. Huang da W, Sherman BT, Lempicki RA. Bioinformatics enrichment tools: paths toward the comprehensive functional analysis of large gene lists. Nucleic Acids Res [Internet]. 2008/11/25. 2009 Jan;37(1):1–13. Available from: https://www.ncbi.nlm.nih.gov/pubmed/19033363

46. Huang da W, Sherman BT, Lempicki RA. Systematic and integrative analysis of large gene lists using DAVID bioinformatics resources. Nat Protoc [Internet]. 2009 Jan 18;4(1):44–57. Available from: https://www.ncbi.nlm.nih.gov/pubmed/19131956

47. Goubau D, der Veen AG, Chakravarty P, Lin R, Rogers N, Rehwinkel J, et al. Mouse superkiller-2-like helicase DDX60 is dispensable for type I IFN induction and immunity to multiple viruses. Eur J Immunol [Internet]. 2015 Dec 12;45(12):3386–403. Available from: https://onlinelibrary.wiley.com/doi/10.1002/eji.201545794

48. Si-Tahar M, Blanc F, Furio L, Chopy D, Balloy V, Lafon M, et al. Protective Role of LGP2 in Influenza Virus Pathogenesis. J Infect Dis [Internet]. 2014 Jul 15;210(2):214–23. Available from: https://academic.oup.com/jid/article-lookup/doi/10.1093/infdis/jiu076

49. François-Newton V, Magno de Freitas Almeida G, Payelle-Brogard B, Monneron

D, Pichard-Garcia L, Piehler J, et al. USP18-Based Negative Feedback Control Is Induced by Type I and Type III Interferons and Specifically Inactivates Interferon α Response. Mossman KL, editor. PLoS One [Internet]. 2011 Jul 14;6(7):e22200. Available from: https://dx.plos.org/10.1371/journal.pone.0022200

50. Li J, Jin K, Li M, Mathy NW, Gong A-Y, Deng S, et al. The host cell long noncoding RNA NR _ 033736 regulates type I interferon-mediated gene transcription and modulates intestinal epithelial anti-Cryptosporidium defense. PLoS Pathogens. 2020.

51. Weese JS, Kenney DG, O'Connor A. Secondary lactose intolerance in a neonatal goat. J Am Vet Med Assoc [Internet]. 2000 Aug;217(3):372–5. Available from: https://www.ncbi.nlm.nih.gov/pubmed/10935043

52. Donnelly MT. Cryptosporidiosis Identified in the Greater Metropolitan St. Louis Area [Internet]. Services MD of H& S, editor. 2010. Available from: https://health.mo.gov/emergencies/ert/alertsadvisories/pdf/HAd8-6-10.pdf

53. Relat RMB, O'Connor RM. Cryptosporidium: host and parasite transcriptome in infection. Curr Opin Microbiol [Internet]. 2020/11/04. 2020 Dec;58:138–45. Available from: https://www.ncbi.nlm.nih.gov/pubmed/33160225

54. O'Connor RM, Burns PB, Ha-Ngoc T, Scarpato K, Khan W, Kang G, et al. Polymorphic Mucin Antigens CpMuc4 and CpMuc5 Are Integral to Cryptosporidium parvum Infection In Vitro. Eukaryot Cell [Internet]. 2009 Apr;8(4):461–9. Available from: https://ec.asm.org/content/8/4/461

55. Lippuner C, Ramakrishnan C, Basso WU, Schmid MW, Okoniewski M, Smith NC,

et al. RNA-Seq analysis during the life cycle of Cryptosporidium parvum reveals significant differential gene expression between proliferating stages in the intestine and infectious sporozoites. Int J Parasitol [Internet]. 2018 May;48(6):413–22. Available from: https://linkinghub.elsevier.com/retrieve/pii/S0020751918300183

56. Amadi B, Mwiya M, Sianongo S, Payne L, Watuka A, Katubulushi M, et al. High dose prolonged treatment with nitazoxanide is not effective for cryptosporidiosis in HIV positive Zambian children: a randomized controlled trial. BMC Infect Dis [Internet]. 2009 Dec 2;9:195. Available from: http://www.ncbi.nlm.nih.gov/pubmed/19954529

57. Amadi B, Mwiya M, Musuku J, Watuka A, Sianongo S, Ayoub A, et al. Effect of nitazoxanide on morbidity and mortality in Zambian children with cryptosporidiosis: a randomized controlled trial. Lancet (London, England) [Internet]. 2002 Nov 2;360(9343):1375–80. Available from: http://www.ncbi.nlm.nih.gov/pubmed/12423984

58. Rossignol JF, Ayoub A, Ayers MS. Treatment of diarrhea caused by Cryptosporidium parvum: a prospective randomized, double-blind, placebo-controlled study of Nitazoxanide. J Infect Dis [Internet]. 2001 Jul 1;184(1):103–6. Available from: http://www.ncbi.nlm.nih.gov/pubmed/11398117

59. Mesev E V., LeDesma RA, Ploss A. Decoding type I and III interferon signalling during viral infection. Nat Microbiol [Internet]. 2019 Jun 1;4(6):914–24. Available from: http://dx.doi.org/10.1038/s41564-019-0421-x

60. Sim CK, Cho YS, Kim BS, Baek I-J, Kim Y-J, Lee MS. 2′–5′ Oligoadenylate

synthetase-like 1 (OASL1) deficiency in mice promotes an effective anti-tumor immune response by enhancing the production of type I interferons. Cancer Immunol Immunother [Internet]. 2016 Jun;65(6):663–75. Available from: http://link.springer.com/10.1007/s00262-016-1830-9

61. Barakat FM, McDonald V, Foster GR, Tovey MG, Korbel DS. Cryptosporidium parvum infection rapidly induces a protective innate immune response involving type I interferon. J Infect Dis [Internet]. 2009;200(10):1548–55. Available from: https://www.ncbi.nlm.nih.gov/pubmed/19821721

62. Heo I, Dutta D, Schaefer DA, Iakobachvili N, Artegiani B, Sachs N, et al. Modelling Cryptosporidium infection in human small intestinal and lung organoids. Nat Microbiol [Internet]. 2018/06/25. 2018 Jul 25;3(7):814–23. Available from: https://www.ncbi.nlm.nih.gov/pubmed/29946163

63. Kang JS, Hwang YS, Kim LK, Lee S, Lee W Bin, Kim-Ha J, et al. OASL1 traps viral RNAs in stress granules to promote antiviral responses. Mol Cells. 2018;41(3):214–23.

64. Zhu J, Zhang Y, Ghosh A, Cuevas RA, Forero A, Dhar J, et al. Antiviral Activity of Human OASL Protein Is Mediated by Enhancing Signaling of the RIG-I RNA Sensor. Immunity [Internet]. 2014;40(6):936–48. Available from: http://dx.doi.org/10.1016/j.immuni.2014.05.007

65. Eskildsen S, Hartmann R, Kjeldgaard NO, Justesen J. Gene structure of the murine 2′-5′-oligoadenylate synthetase family. Cell Mol Life Sci [Internet]. 2002 Jul 1;59(7):1212–22. Available from: http://link.springer.com/10.1007/s00018-002-8499-2

66. Lee MS, Kim B, Oh GT, Kim Y-J. OASL1 inhibits translation of the type I interferon–regulating transcription factor IRF7. Nat Immunol [Internet]. 2013 Apr 17;14(4):346–55. Available from: http://www.nature.com/articles/ni.2535

67. Mavrommatis E, Fish EN, Platanias LC. The Schlafen Family of Proteins and Their Regulation by Interferons. J Interf Cytokine Res [Internet]. 2013 Apr;33(4):206–10. Available from: https://www.ncbi.nlm.nih.gov/pubmed/23570387

68. Katsoulidis E, Carayol N, Woodard J, Konieczna I, Majchrzak-Kita B, Jordan A, et al. Role of Schlafen 2 (SLFN2) in the Generation of Interferon α-induced Growth Inhibitory Responses. J Biol Chem [Internet]. 2009/07/10. 2009 Sep 11;284(37):25051–64. Available from: https://www.ncbi.nlm.nih.gov/pubmed/19592487

69. Fischietti M, Arslan AD, Sassano A, Saleiro D, Majchrzak-Kita B, Ebine K, et al. Slfn2 Regulates Type I Interferon Responses by Modulating the NF-κB Pathway. Mol Cell Biol [Internet]. 2018/07/30. 2018 Jun 4;38(16). Available from: https://www.ncbi.nlm.nih.gov/pubmed/29866656

70. Neumann B, Zhao L, Murphy K, Gonda TJ. Subcellular localization of the Schlafen protein family. Biochem Biophys Res Commun [Internet]. 2008/03/18. 2008;370(1):62–6. Available from: https://www.ncbi.nlm.nih.gov/pubmed/18355440

71. van Zuylen WJ, Garceau V, Idris A, Schroder K, Irvine KM, Lattin JE, et al. Macrophage Activation and Differentiation Signals Regulate Schlafen-4 Gene Expression: Evidence for Schlafen-4 as a Modulator of Myelopoiesis. Poh LNF,

editor. PLoS One [Internet]. 2011/01/07. 2011 Jan 7;6(1):e15723. Available from: https://www.ncbi.nlm.nih.gov/pubmed/21249125

72. Kirkpatrick BD, Daniels MM, Jean SS, Pape JW, Karp C, Littenberg B, et al. Cryptosporidiosis stimulates an inflammatory intestinal response in malnourished Haitian children. J Infect Dis [Internet]. 2002 Jul 1;186(1):94–101. Available from: http://www.ncbi.nlm.nih.gov/pubmed/12089667

73. Pantenburg B, Dann SM, Wang H-C, Robinson P, Castellanos-Gonzalez A, Lewis DE, et al. Intestinal immune response to human Cryptosporidium sp. infection. Infect Immun [Internet]. 2008 Jan;76(1):23–9. Available from: http://www.ncbi.nlm.nih.gov/pubmed/17967863

74. Kaushik K, Khurana S, Wanchu A, Malla N. Lymphoproliferative and cytokine responses to Cryptosporidium parvum in patients coinfected with C. parvum and human immunodeficiency virus. Clin Vaccine Immunol [Internet]. 2009 Jan;16(1):116–21. Available from: http://www.ncbi.nlm.nih.gov/pubmed/19020105

75. Campbell LD, Stewart JN, Mead JR. Susceptibility to Cryptosporidium parvum infections in cytokine- and chemokine-receptor knockout mice. J Parasitol [Internet]. 2002 Oct;88(5):1014–6. Available from: http://www.ncbi.nlm.nih.gov/pubmed/12435147

76. Raabis SM, Ollivett TL, Cook ME, Sand JM, McGuirk SM. Health benefits of orally administered anti-IL-10 antibody in milk-fed dairy calves. J Dairy Sci [Internet]. 2018 Aug;101(8):7375–82. Available from: http://www.ncbi.nlm.nih.gov/pubmed/29778481

77. Laurent F, Kagnoff MF, Savidge TC, Naciri M, Eckmann L. Human intestinal epithelial cells respond to Cryptosporidium parvum infection with increased prostaglandin H synthase 2 expression and prostaglandin E2 and F2alpha production. Infect Immun [Internet]. 1998 Apr;66(4):1787–90. Available from: http://www.ncbi.nlm.nih.gov/pubmed/9529115

78. Gookin JL, Duckett LL, Armstrong MU, Stauffer SH, Finnegan CP, Murtaugh MP, et al. Nitric oxide synthase stimulates prostaglandin synthesis and barrier function in C. parvum-infected porcine ileum. Am J Physiol Gastrointest Liver Physiol [Internet]. 2004 Sep;287(3):G571-81. Available from: http://www.ncbi.nlm.nih.gov/pubmed/15155179

79. Olsen L, Åkesson CP, Storset AK, Lacroix-Lamandé S, Boysen P, Metton C, et al. The early intestinal immune response in experimental neonatal ovine cryptosporidiosis is characterized by an increased frequency of perforin expressing NCR1(+) NK cells and by NCR1(-) CD8(+) cell recruitment. Vet Res [Internet]. 2015 Mar 11;46(1):28. Available from: http://www.ncbi.nlm.nih.gov/pubmed/25890354

80. Lüder CGK, Gross U, Lopes MF. Intracellular protozoan parasites and apoptosis: diverse strategies to modulate parasite-host interactions. Trends Parasitol [Internet]. 2001 Oct;17(10):480–6. Available from: http://www.ncbi.nlm.nih.gov/pubmed/11587962

81. Reijasse D, Patey-Mariaud de Serre N, Canioni D, Huerre M, Haddad E, Leborgne M, et al. Cytotoxic T cells in AIDS colonic cryptosporidiosis. J Clin Pathol [Internet]. 2001 Apr;54(4):298–303. Available from:

http://www.ncbi.nlm.nih.gov/pubmed/11304847

82. Pantenburg B, Castellanos-Gonzalez A, Dann SM, Connelly RL, Lewis DE, Ward HD, et al. Human CD8(+) T cells clear Cryptosporidium parvum from infected intestinal epithelial cells. Am J Trop Med Hyg [Internet]. 2010 Apr;82(4):600–7. Available from: http://www.ncbi.nlm.nih.gov/pubmed/20348507

83. Korbel DS, Barakat FM, Di Santo JP, McDonald V. CD4+ T cells are not essential for control of early acute Cryptosporidium parvum infection in neonatal mice. Infect Immun [Internet]. 2011 Apr;79(4):1647–53. Available from: http://www.ncbi.nlm.nih.gov/pubmed/21282414

84. Bandini G, Haserick JR, Motari E, Ouologuem DT, Lourido S, Roos DS, et al. O-fucosylated glycoproteins form assemblies in close proximity to the nuclear pore complexes of Toxoplasma gondii. Proc Natl Acad Sci U S A [Internet]. 2016;113(41):11567–72. Available from: http://www.ncbi.nlm.nih.gov/pubmed/27663739

85. Lopaticki S, Yang ASP, John A, Scott NE, Lingford JP, O'Neill MT, et al. Protein O-fucosylation in Plasmodium falciparum ensures efficient infection of mosquito and vertebrate hosts. Nat Commun [Internet]. 2017;8(1):561. Available from: http://dx.doi.org/10.1038/s41467-017-00571-y

86. Bandini G, Leon DR, Hoppe CM, Zhang Y, Agop-Nersesian C, Shears MJ, et al. O-Fucosylation of thrombospondin-like repeats is required for processing of microneme protein 2 and for efficient host cell invasion by Toxoplasma gondii tachyzoites. J Biol Chem [Internet]. 2019;294(6):1967–83. Available from: http://www.ncbi.nlm.nih.gov/pubmed/30538131

87. Martínez-Ocaña J, Maravilla P, Olivo-Díaz A. Interaction between human mucins and parasite glycoproteins: the role of lectins and glycosidases in colonization by intestinal protozoa. Rev Inst Med Trop Sao Paulo [Internet]. 2020;62(64):1–10. Available from: http://www.scielo.br/scielo.php?script=sci_arttext&pid=S0036-46652020000100229&tlng=en

88. O'Connor RM, Wanyiri JW, Cevallos AM, Priest JW, Ward HD. Cryptosporidium parvum glycoprotein gp40 localizes to the sporozoite surface by association with gp15. Mol Biochem Parasitol [Internet]. 2007 Nov;156(1):80–3. Available from: https://linkinghub.elsevier.com/retrieve/pii/S0166685107002137

89. Barnes DA, Bonnin A, Huang J-X, Gousset L, Wu J, Gut J, et al. A novel multi-domain mucin-like glycoprotein of Cryptosporidium parvum mediates invasion1Note: Nucleotide sequence data reported in this paper are available in the EMBL, GenBank™, and DDJB databases under the accession number AF068065.1,2A portion of the a. Mol Biochem Parasitol [Internet]. 1998 Oct;96(1–2):93–110. Available from: https://linkinghub.elsevier.com/retrieve/pii/S0166685198001194

90. Liu S, Roellig DM, Guo Y, Li N, Frace MA, Tang K, et al. Evolution of mitosome metabolism and invasion-related proteins in Cryptosporidium. BMC Genomics. 2016;17(1):1–16.

91. Xu Z, Guo Y, Roellig DM, Feng Y, Xiao L. Comparative analysis reveals conservation in genome organization among intestinal Cryptosporidium species and sequence divergence in potential secreted pathogenesis determinants among major human-infecting species. BMC Genomics. 2019;20(1):1–15.

92. Denkers EY, Gazzinelli RT, Hieny S, Caspar P, Sher A. Bone marrow macrophages process exogenous Toxoplasma gondii polypeptides for recognition by parasite-specific cytolytic T lymphocytes. J Immunol [Internet]. 1993;150(2):517–26. Available from: https://www.jimmunol.org/content/150/2/517

93. Andrews S.; S Bittencourt a. FastQC: a quality control tool for high throughput sequence data – ScienceOpen [Internet]. Version 0. Babraham Institute. 2010. Available from: http://www.bioinformatics.babraham.ac.uk/projects/fastqc/

94. Bolger AM, Lohse M, Usadel B. Trimmomatic: a flexible trimmer for Illumina sequence data. Bioinformatics [Internet]. 2014/04/01. 2014 Aug 1;30(15):2114–20. Available from: https://www.ncbi.nlm.nih.gov/pubmed/24695404

95. Dobin A, Davis CA, Schlesinger F, Drenkow J, Zaleski C, Jha S, et al. STAR: ultrafast universal RNA-seq aligner. Bioinformatics [Internet]. 2012/10/25. 2013 Jan;29(1):15–21. Available from: https://www.ncbi.nlm.nih.gov/pubmed/23104886

96. Dobin A, Gingeras TR. Mapping RNA-seq Reads with STAR. Curr Protoc Bioinforma [Internet]. 2015 Sep 3;51(1):11.14.1-11.14.19. Available from: https://pubmed.ncbi.nlm.nih.gov/26334920

97. Li B, Dewey CN. RSEM: accurate transcript quantification from RNA-Seq data with or without a reference genome. BMC Bioinformatics [Internet]. 2011/08/06. 2011 Dec 4;12(1):323. Available from: https://bmcbioinformatics.biomedcentral.com/articles/10.1186/1471-2105-12-323

98. Soneson C, Love MI, Robinson MD. Differential analyses for RNA-seq: transcript-level estimates improve gene-level inferences. F1000Research [Internet].

2015/12/30. 2016 Feb 29;4:1521. Available from: https://www.ncbi.nlm.nih.gov/pubmed/26925227

99. Love MI, Huber W, Anders S. Moderated estimation of fold change and dispersion for RNA-seq data with DESeq2. Genome Biol [Internet]. 2014 Dec 5;15(12):550. Available from: https://www.ncbi.nlm.nih.gov/pubmed/25516281

Figures

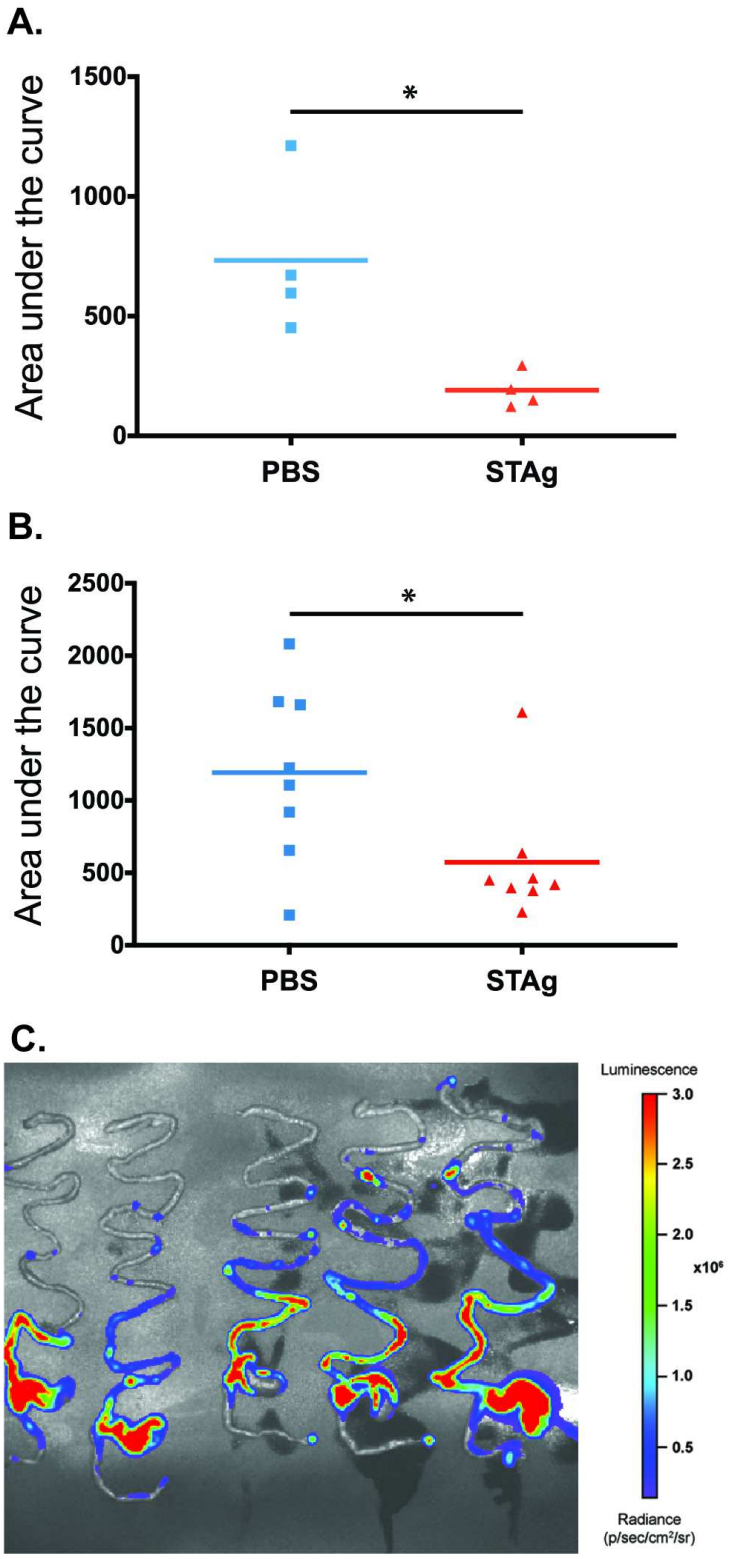

Figure 1

Infection time course of C. parvum infected mice treated with STAg or PBS. (A). The area under the curve of treated mice in experiment #1 over 15 days of infection; *p=0.03, Oocyst shedding calculated by qPCR, as described in the methods section. (B). The area under the curve of treated mice in experiment #2 over

15 days of infection; *p=0.034, Oocyst shedding calculated by expression of nanoLuciferase, as described in the methods section. (C) Bioluminescent imaging of C. parvum in mice small intestine: the small intestine of mice infected 9 dpi with Nluc C. parvum Iowa II strain at 1x105 showing a higher abundance in the ileum and cecum regions. Radiance scale bar (p/sec/cm2/s).

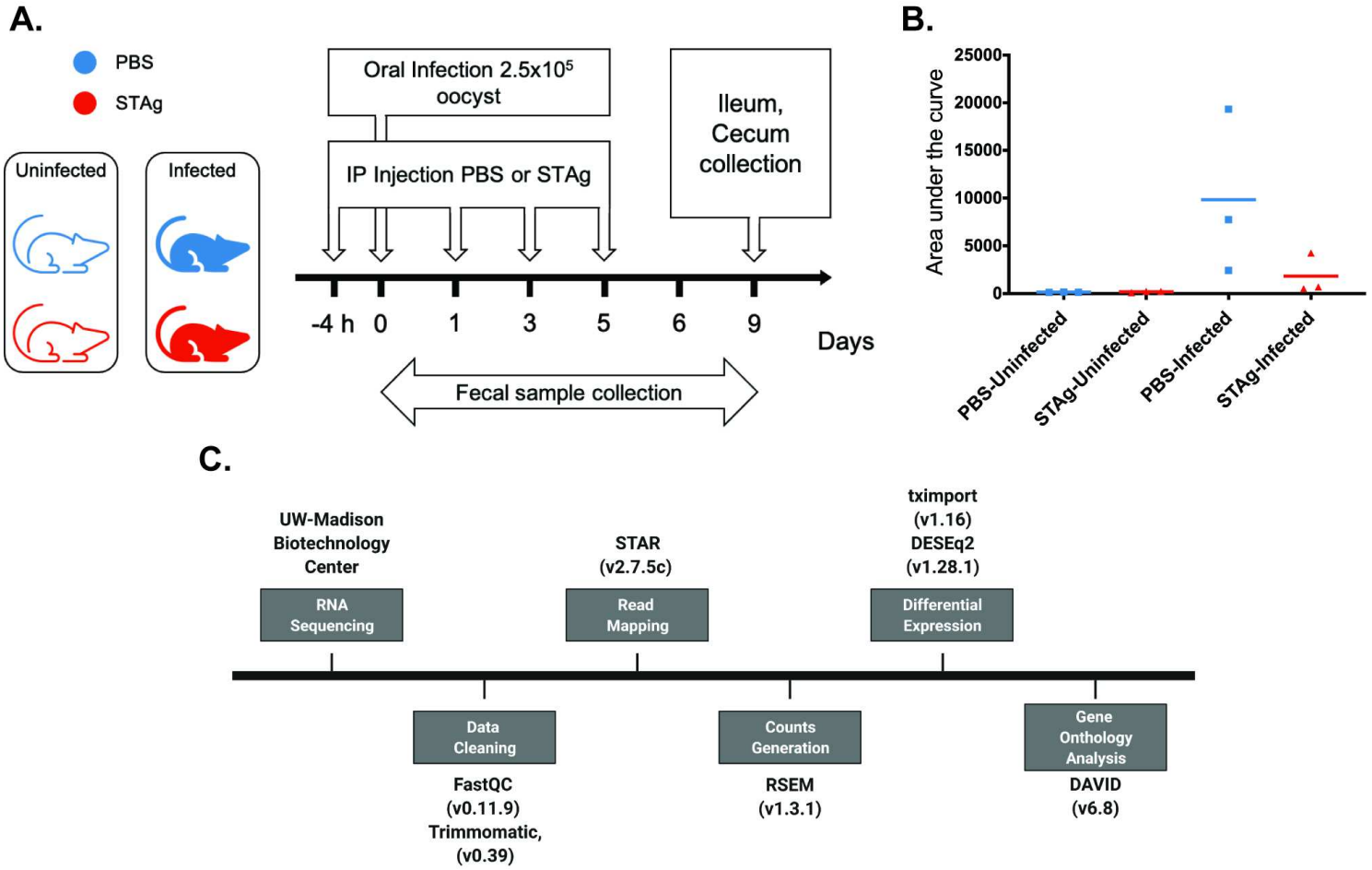

Figure 2

Mice Experimental Design and analysis for RNA sequencing. (A). For the RNAseq analysis, 12 mice, 6 infected and 6 non-infected were treated with PBS or STAg. The treatment was administered 4 hours prior to infection (2.5x105 Nluc C. parvum Iowa II strain oocyst by oral gavage) and 1, 3, and 5 days post-infection. Fecal samples were collected every other day and infection quantified by nanoLuciferase expression. Mice were euthanized on 9 dpi and ileum and cecum samples were collected. (B). Oocyst shedding calculated by expression of nanoLuciferase, as described in the methods section, and area under the curve calculated over 9 dpi. Each square (PBS) or each triangle (STAg) represents a mouse. Statistic differences were analyzed by t-test using GraphPad PRISM and the mean of each group is represented 21 with a line. (C). RNA sequencing analysis flowchart listing the programs and packages utilized for reading and analysis. Versions used are indicated in parenthesis.

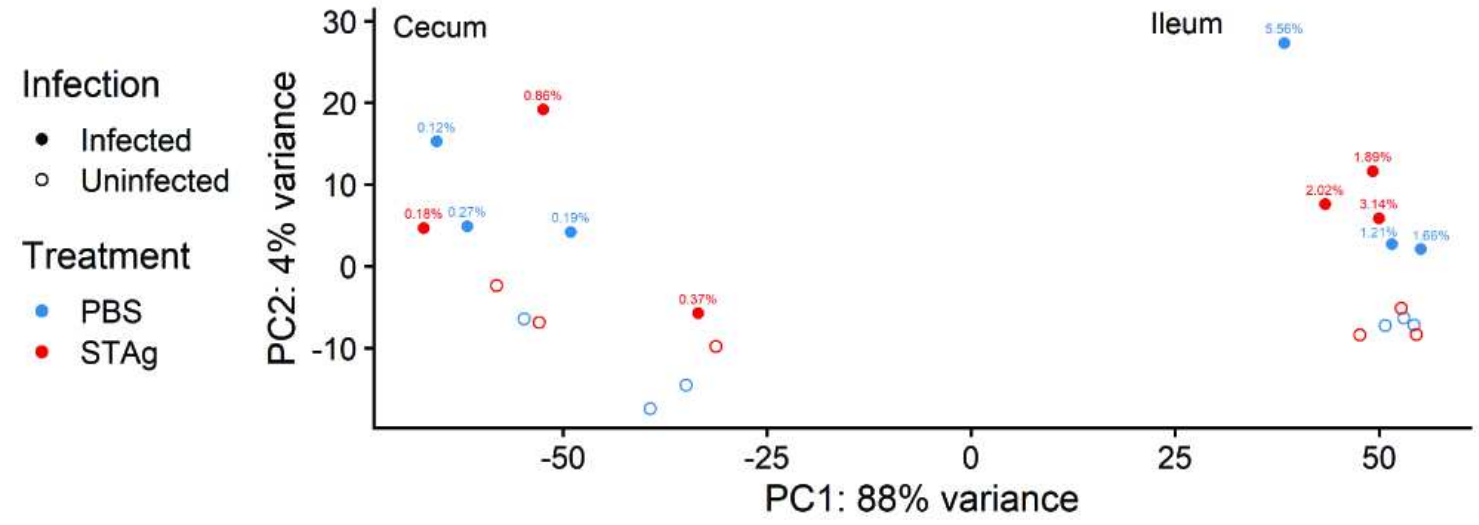

Figure 3

Principal Component Analysis (PCA) of ileum and cecum samples. PCA plot from normalized values calculated by DESeq2. Mapping of the cecum and ileum intestinal section to Mus musculus genome. Symbol filling represents C. parvum infection status: Uninfected (open); Infected (filled). Symbol color represents treatment: control treatment PBS (blue); Soluble T. gondii antigen, STAg (red). The text above individual mice corresponds to the percent of reads uniquely mapped to the C. parvum genome.

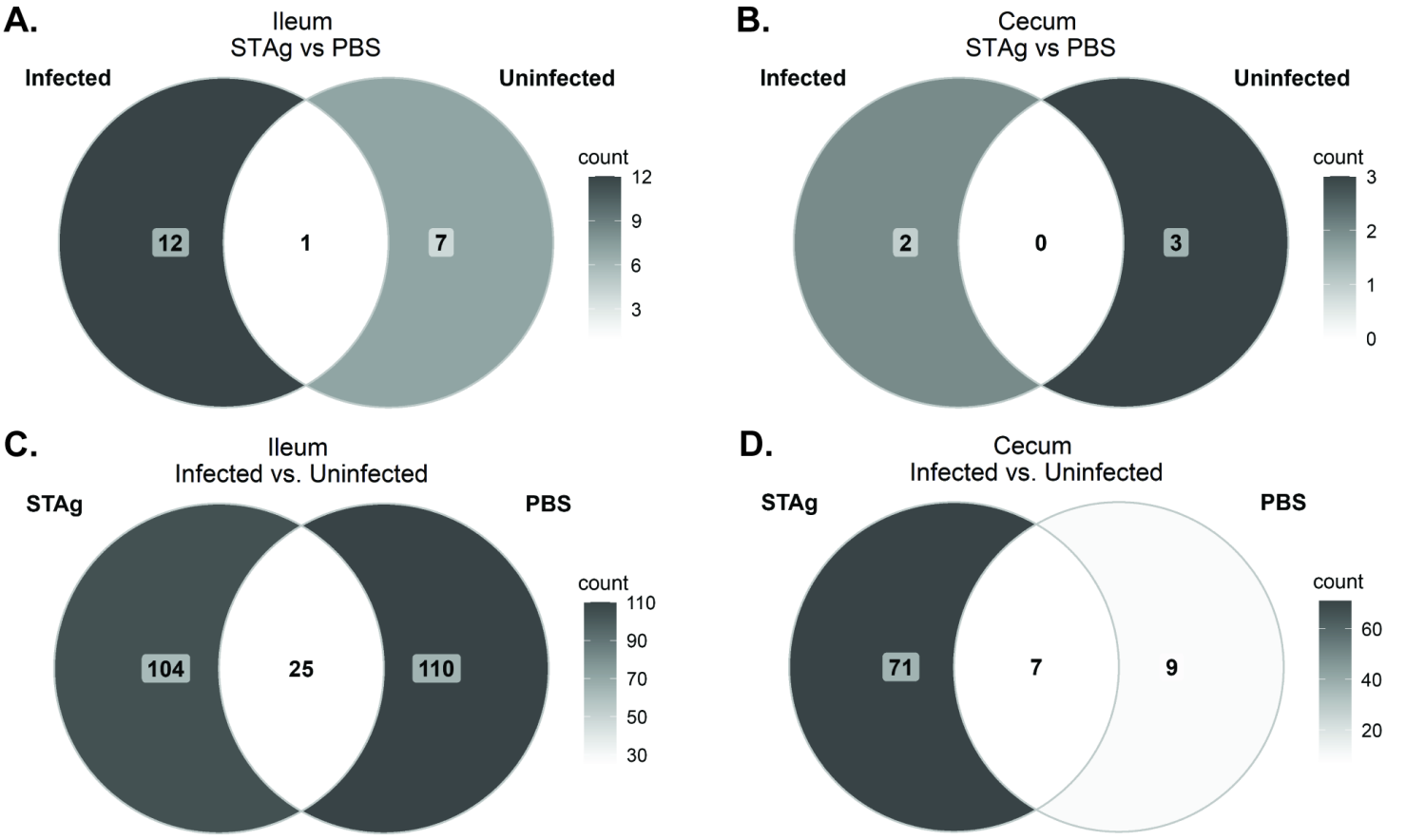

Figure 4

Host Differential expressed genes by treatment, infectious status, and tissue. (A). Host genes with significantly different abundance when infection status was constant, and treatment was compared in the ileum (comparisons 1 and 2) and (B) cecum (comparisons 3 and 4). (C). Host genes with significantly different abundance when treatment was constant and infection status was compared in the ileum (comparisons 5 and 6) and (D) cecum (comparison 7 and 8). Significant calls had a < 0.05 padj value and a > 2 absolute log2fold change. Shared sets of significant calls are represented by overlapping regions in the diagram. Color scale represents a higher number of calls as darker shades of grey. The specifics of each mouse group can be found in the table (Tables S2 and S3). Visualization of all possible comparisons can be found in Figure S1 and Figure S2.

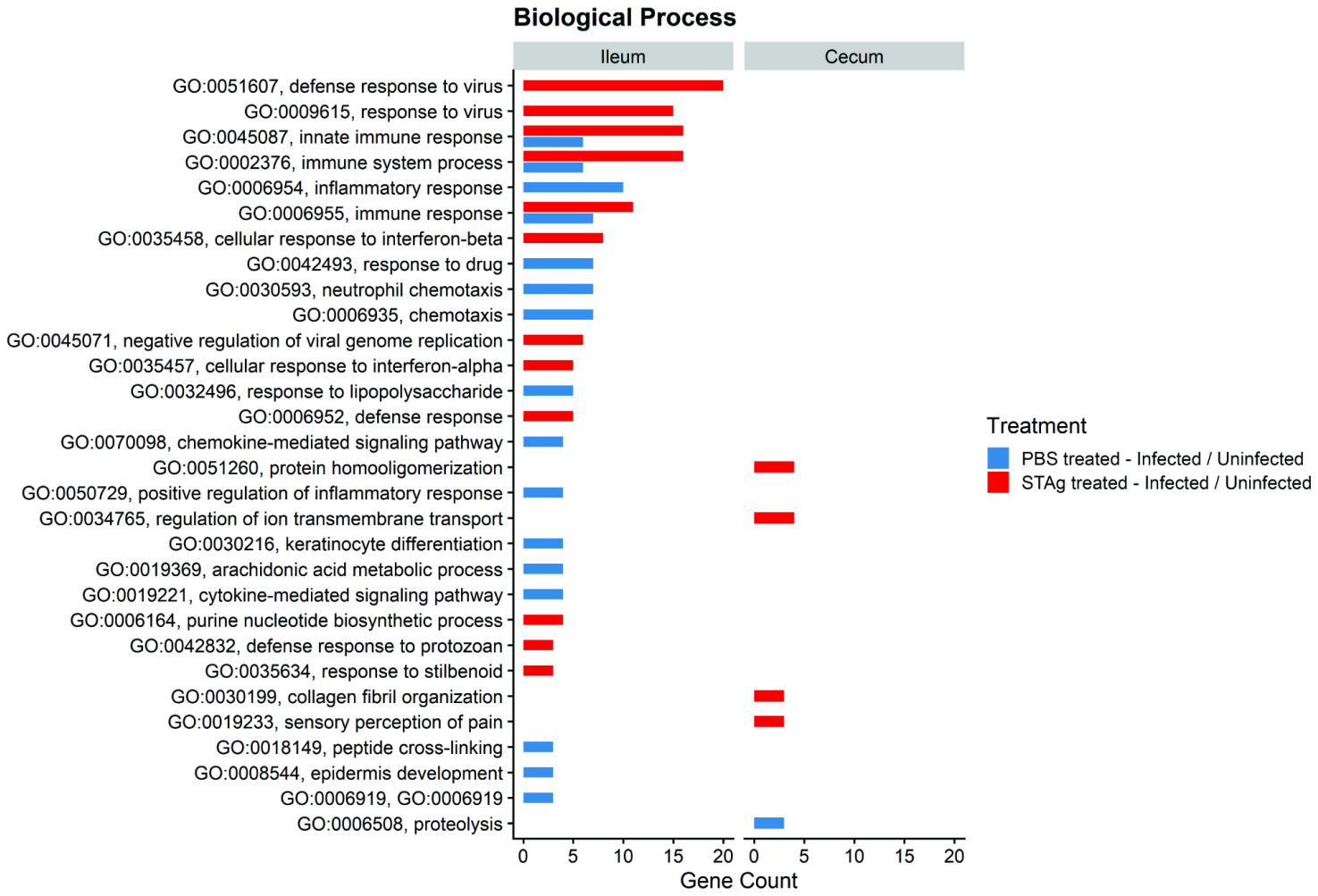

Figure 5

Host gene ontology (GO) of biological process (BP) in STAg and PBS treated mice. Differentially expressed genes (DEGs) in comparisons 5-8 were analyzed for gene ontology enrichment of biological process (BP), using the Database for Annotation, Visualization, and Integrated Discovery (DAVID, v6.8). Only GO terms populated by 3 or more DEGs were included in these visualizations ($p < 0.05$). Bar filling color represents treatment: control treatment PBS (blue); Soluble T. gondii antigen, STAg (red).

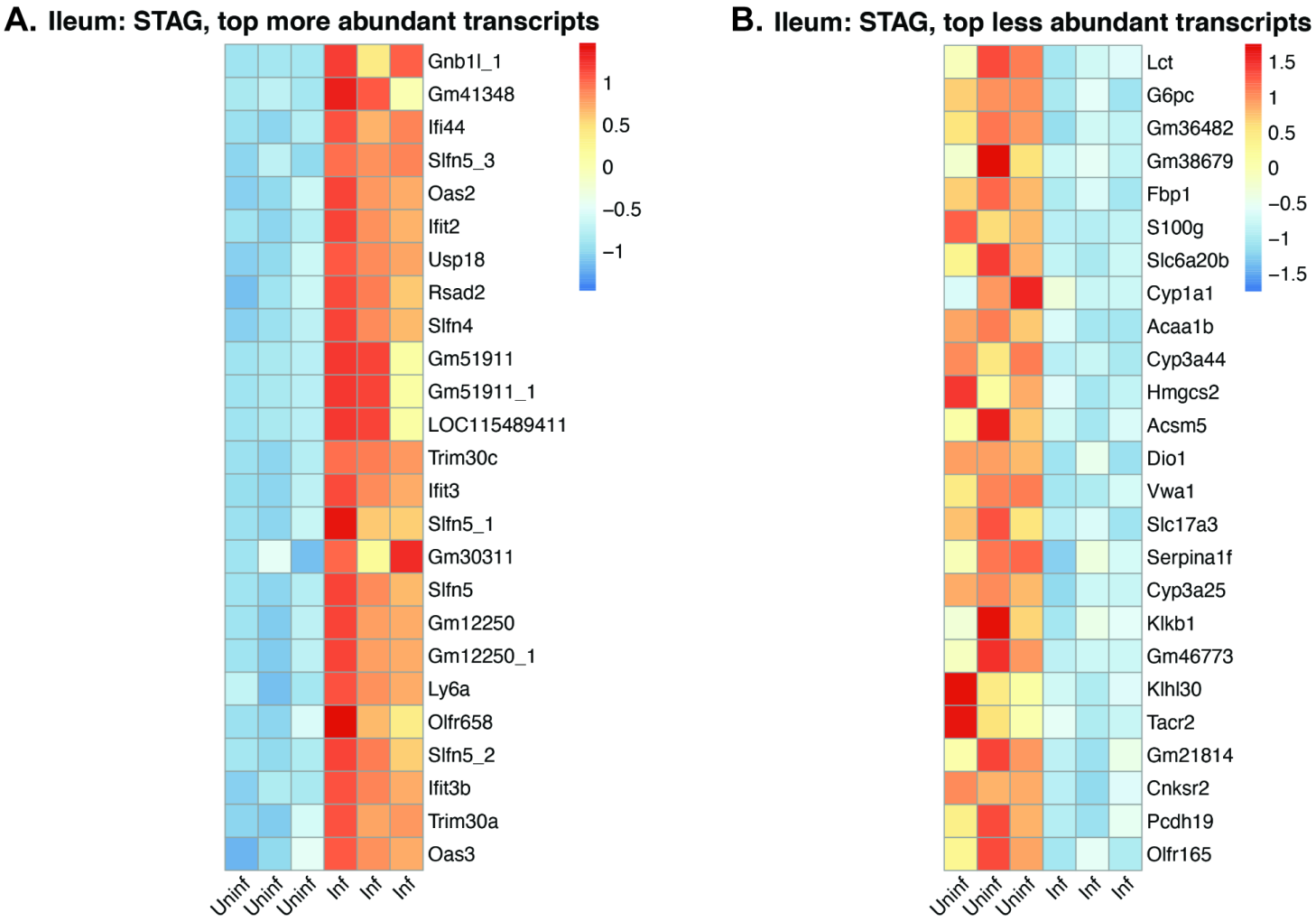

Figure 6

Heatmap of differentially expressed genes in the ileum of mice treated with STAg (comparison 5). The top 25 more (A) and less (B) abundant transcripts (ranked by log2 fold change). Each column represents a biological replicate.

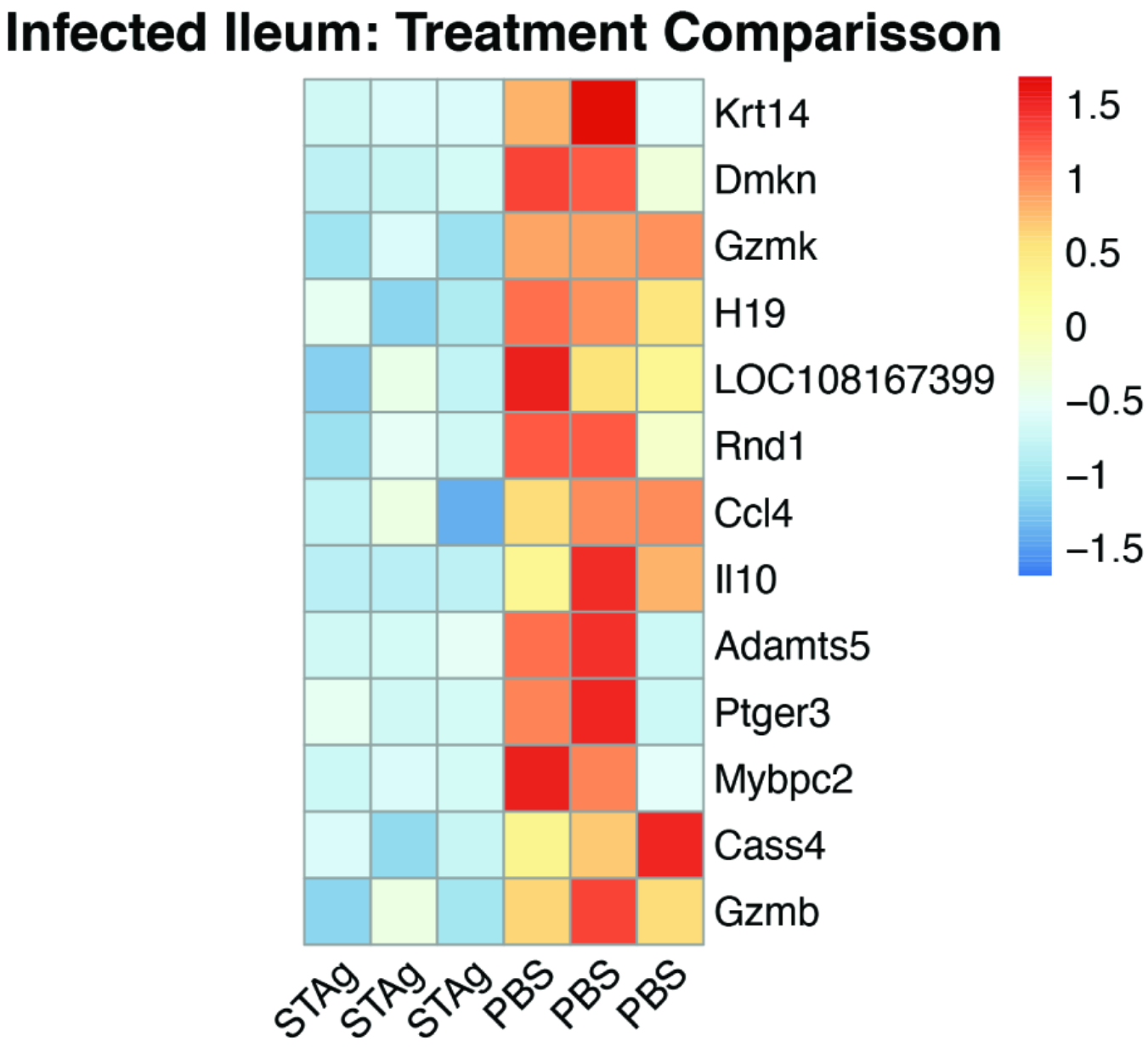

Figure 7

Heatmap of differentially expressed genes in the ileum of infected mice treated with STAg or PBS. 13 genes (ranked by log2 fold change) were found to be differentially expressed in the ileum between infected mice treated with PBS or STAg. Each column represents a biological replicate.

Supplementary Files

This is a list of supplementary files associated with this preprint. Click to download.

- Table1.docx

- Table2.docx
- Table3.docx
- Supplementalfile1.csv
- Supplementalfile8.csv
- Supplementalfile6.csv
- Supplementalfile2.csv
- Supplementalfile11.csv
- Supplementalfile3.csv
- Supplementalfile7.csv
- Supplementalfile4.csv
- Supplementalfile12.csv
- FIGS1.tif
- TableS1.docx
- TableS2.docx
- FIGS2.tif
- TableS3.docx
- FIGS3.tif
- FIGS1.tif
- FIGS4.tif
- FIGS5.tif
- FIGS2.tif
- FIGS6.tif
- FIGS3.tif
- FIGS4.tif
- Supplementalfile1.csv
- Supplementalfile10.csv
- FIGS6.tif
- FIGS5.tif
- Supplementalfile11.csv
- Supplementalfile12.csv
- Supplementalfile5.csv
- Supplementalfile9.csv
- Supplementalfile2.csv
- Supplementalfile10.csv

- Supplementalfile3.csv
- Supplementalfile4.csv
- Supplementalfile5.csv
- Supplementalfile6.csv
- Supplementalfile7.csv
- Supplementalfile8.csv
- Supplementalfile9.csv
- TableS1.docx
- TableS2.docx
- TableS3.docx